frontiers in Physics

REVIEW
published: 13 March 2020
doi: 10.3389/fphy.2020.00022

Printable Organic Semiconductors for Radiation Detection: From Fundamentals to Fabrication and Functionality

Matthew J. Griffith[1,2,3]*, *Sophie Cottam*[2], *Joshua Stamenkovic*[2], *Jessie A. Posar*[4] and *Marco Petasecca*[4]

[1] Faculty of Science, School of Mathematical and Physical Sciences, University of Newcastle, Callaghan, NSW, Australia, [2] Centre for Organic Electronics, University of Newcastle, Callaghan, NSW, Australia, [3] School of Aerospace, Mechanical and Mechatronic Engineering, The University of Sydney, Camperdown, NSW, Australia, [4] Centre for Medical Radiation Physics, University of Wollongong, Wollongong, NSW, Australia

The deployment of organic semiconducting materials for radiation detection is an emerging and highly attractive area of materials science research. These organic materials offer the enticing vision of technologies created from low-cost materials that can be printed on-demand with a range of different tailored optoelectronic functionalities. An explosion in the number of available materials, improved functionality of materials, and sophistication of solution-based device fabrication techniques for organic semiconductors in recent years have led to considerable opportunities for the utilization of organic materials in the detection of ionizing radiation. While the potential of organic semiconducting materials for low-cost radiation detection is clear, transitioning these printable materials to a commercial reality presents a significant scientific challenge. In this work, we provide a comprehensive analysis of the use of organic semiconductors for radiation detection. We discuss the fundamental physics of these materials and how their conduction mechanisms, including charge generation and charge transport, differ significantly from established inorganic semiconductors. Various strategies employed to control the nanostructure in organic semiconductors to optimize charge generation and transport for radiation detection are discussed. We provide insights into the strategies employed to fabricate organic semiconducting devices at industrially relevant scales using roll-to-roll solution processing and finally discuss existing examples of organic semiconducting materials utilized in the radiation detection arena.

Keywords: nanostructure, organic semiconductors, printing, radiation detection, sensing

OPEN ACCESS

Edited by:
Beatrice Fraboni,
University of Bologna, Italy

Reviewed by:
Alessandro Tricoli,
Brookhaven National Laboratory (DOE), United States
Sally Seidel,
University of New Mexico, United States

***Correspondence:**
Matthew J. Griffith
matthew.griffith@sydney.edu.au

Specialty section:
This article was submitted to Radiation Detectors and Imaging, a section of the journal Frontiers in Physics

Received: *16 October 2019*
Accepted: *27 January 2020*
Published: *13 March 2020*

Citation:
Griffith MJ, Cottam S, Stamenkovic J, Posar JA and Petasecca M (2020) Printable Organic Semiconductors for Radiation Detection: From Fundamentals to Fabrication and Functionality. Front. Phys. 8:22. doi: 10.3389/fphy.2020.00022

INTRODUCTION

The utilization of ionizing radiation in many aspects of modern society has risen dramatically in the past few decades, leading to a growing demand for new innovative and low-cost electronic materials that can detect this radiation. Traditionally, radiation detectors are fabricated from inorganic semiconducting materials such as silicon, germanium, cadmium telluride, cadmium zinc telluride, or mercury iodide, which either directly convert ionizing radiation into an electrical signal or detect the radiation-induced photoluminescence of a scintillation crystal [1, 2]. However, these rigid materials, while exhibiting impressive detector performances, do suffer from some

substantial limitations. Such limitations include difficulty in processing into large-area pixelated detector matrixes, an inability to conform to various complex curved shapes such as the human body, and the requirement for calibration of correction factors to measure the radiation dose delivered to biological species because the device materials do not have a water-equivalent density [3, 4]. A radiation detection system that could address such limitations would have wide-ranging applications across areas including radiation protection, dosimetry measurements for radiotherapy, X-ray imaging in diagnostic radiology, or personal health monitoring in a range of high-risk industries [5, 6].

Demand from such applications has led to increasing interest in organic semiconductors (OSCs) as a particularly attractive class of materials for radiation detection [7]. OSC materials offer the exciting prospect of combining the electronic advantages of semiconducting substrates with the chemical and mechanical benefits of organic compounds such as plastics. The suitability of OSC materials for this purpose arises from the ability to easily modify their chemical, physical, and electronic properties and control their film-forming mechanisms through conventional wet chemistry [8]. Furthermore, because these materials are composed almost entirely of carbon, hydrogen, and oxygen, they have a response to radiation that closely mimics that of water, thus providing a key advantage for radiation dosimetry [9, 10]. Finally, organic materials, in direct contrast to their inorganic counterparts, can be dissolved in solutions to create inks. This property opens up avenues for printing devices directly onto mechanically flexible substrates at high speeds across large areas using cheap roll-to-roll (R2R) processing techniques (**Figure 1**) [11–13]. However, realization of the potential for OSC materials in such applications requires two critical parallel developments. First, innovative manufacturing techniques that are faster, cheaper, and more eco-friendly than conventional methods must be developed [14–17]. Simultaneously, new electronic materials must be developed that are compatible with these solution-based manufacturing techniques and allow manipulation of the nanoscale architecture of multilayer thin films to create highly functional electronic devices [18–21].

While the potential of OSCs for low-cost radiation detection is clear, transitioning these printable materials to a commercial reality presents a significant scientific challenge. Through intense research in OSC materials for applications in solar cells [22–25], transistors [26–29], and sensor devices [30–32], it has become clear that the photophysics of charge generation and transport are unique and do not occur with the same efficiency as in inorganic semiconductors. It is therefore critical to create a highly precise nanoscale ordering of the materials across large size scales to compensate for these deficiencies and allow the devices to function efficiently. This precise control of nanoscale morphology in multilayer OSC devices is typically achieved with various carefully calibrated laboratory fabrication and processing technique [33]. However, controlling the material nanoscale structure and morphology across large areas during the printing fabrication processes required for mass manufacture remains a significant challenge due to the crude thermodynamic levers available in the printing process [34]. In this article, we will provide an overview of the fundamental physics of OSC materials and then discuss their recent applications in radiation detection. We provide insight into various materials and fabrication innovations that are targeted toward creating, maintaining, and characterizing the nanoscale structure of OSC materials for radiation detection during large area printing fabrication.

ORGANIC SEMICONDUCTORS: FUNDAMENTAL PHOTOPHYSICS

An essential requirement for electrical conductivity in a material system is the presence of delocalized electrons that can receive energy from an external field. Organic semiconductors, that is, those materials whose chemical structure is predominantly based on the element carbon, achieve such delocalization through a π-conjugated network that connects molecules as subunits of an organic solid. A single carbon atom is described by the electronic configuration $1s^2 2s^2 2p^2$, a notation that denotes the occupation of electrons in various atomic orbitals in the atom. From this electronic configuration, it becomes clear that the *s*-orbitals of the first and second shells are both fully occupied by two electrons, while the two remaining electrons are found distributed across two of the three degenerate *p*-orbitals (which can host up to a maximum of six electrons). When neighboring carbon atoms in a molecule form chemical bonds with each other, the shared electron density is distributed into hybrid orbitals formed by the interference between the C2*s* and C2*p* atomic orbitals to maximize the spatial separation of the electrons from each other as per the valence shell electron pair repulsion theory (VSEPR) [35].

For a double bond between two carbon atoms in a solid, each individual atom has only three neighbors, and thus, one electron is provided by the *s*-orbital and two by the *p*-orbitals so that three new sp^2 hybridized orbitals are created. These hybrid orbitals lie in a plane and adopt the geometry of an equilateral triangle. The remaining *p*-orbital from the carbon atom ($2p_z$) is not hybridized, and its axis is perpendicular to the plane in which the hybridized sp^2 orbitals lie (**Figure 2**). The carbon atoms can then form three σ-bonds with neighboring carbon atoms through sharing of electrons in the sp^2 orbitals, and a single π-bond with one neighboring atom through sharing of the electrons in the $2p_z$ orbitals [36]. As this concept is extended to a π-conjugated network containing an increasing number of carbon atoms, the $2p_z$ orbitals of each atom overlap through linear superposition to create a single molecular orbital with delocalized electron density across the entire molecule. It is the interaction of these π electrons that dictates the electronic characteristics of the OSC. The energy levels become closely spaced as the OSC conjugation length increases, resulting in "band" structures similar to that observed in inorganic solid-state semiconductors, where the analog of the valence band is now the highest occupied molecular orbital (HOMO, or π-orbital) and the analog to the conduction band is the lowest unoccupied molecular orbital (LUMO, or π^*-orbital) (**Figure 2**) [37]. However, unlike inorganic semiconductors, the primary photoexcited state occurs as a bound electron–hole pair (exciton)

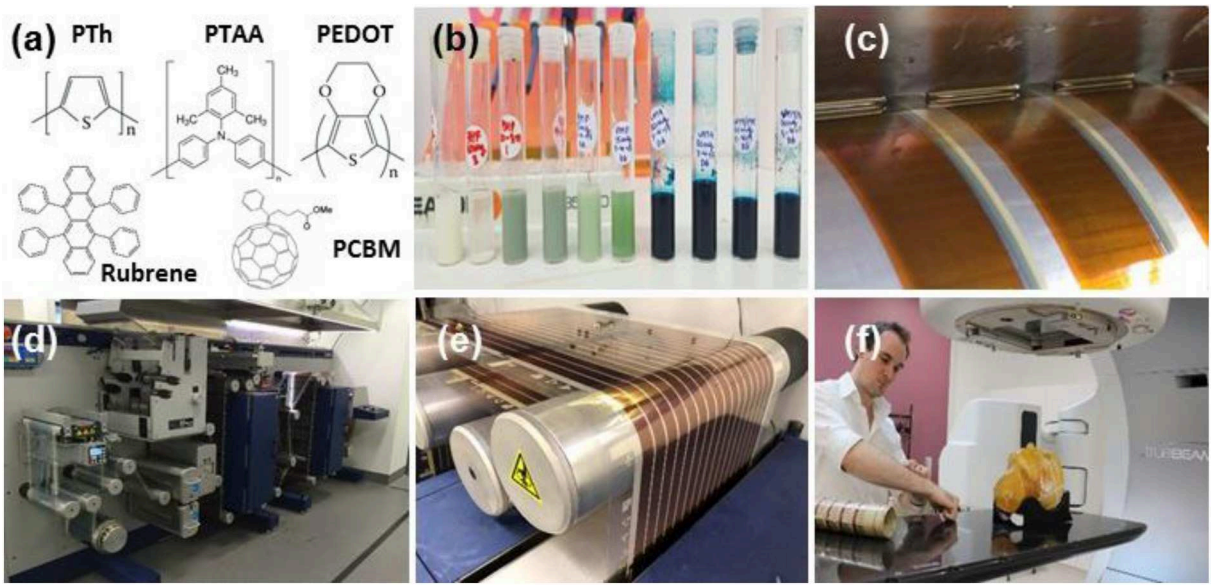

FIGURE 1 | (a) Chemical structure of some organic semiconductors (OSCs) used to detect radiation [PTh, poly(thiophene); PTAA, poly(triarylamine); PEDOT, poly(ethylenedioxythiophene); Rubrene; PCBM, phenyl-C_{61}-butyric acid methyl ester). **(b)** several different organic scintillator and semiconductor materials dissolved into printable inks. **(c)** Image of a dielectric ink being printed onto a semiconducting polymer for radiation detectors. **(d)** A roll-to-roll coating machine printing OSC inks. **(e)** An image of large area organic semiconducting materials printed at industrial scale. **(f)** Printed flexible organic radiation detectors fabricated at the University of Newcastle's Center for Organic Electronics. The authors have confirmed that any identifiable participants in this study have given their consent for publication.

rather than free charge carriers. Furthermore, the transport of charge carriers cannot be understood with a model of band transport due to the weak interaction among π-orbitals. Each of these features becomes important when considering either indirect ionizing radiation detection (high energy particle interacting with a scintillating material, which produces optical photons), where photoexcitation of the OSC is critical, or direct ionizing detection of radiation (high energy particle interacts directly with the OSC substrate), where the transport properties are essential. It is therefore worth considering how both charge generation and charge transport are unique in OSCs to understand how to optimize the use of these materials for ionizing radiation detection.

Charge Generation

The primary photoexcitation process in all semiconducting materials involves the conversion of incident radiation into an electron–hole pair in the excited state of the absorbing material. Efficient detection of the incident radiation requires separation of the photogenerated electron–hole pair into dissociated free charge carriers with a high quantum yield and minimal loss of free energy. To achieve such free carrier separation, the electron–hole pair must overcome their mutual Coulomb attraction potential, V:

$$V = \frac{e^2}{4\pi\varepsilon_r\varepsilon_0 r} \quad (1)$$

where e is the charge of an electron, ε_r is the dielectric constant of the semiconducting material, ε_0 is the permittivity of free space, and r is the electron–hole separation distance. In traditional inorganic semiconductors, the dielectric constant is high (for instance, ε_r for silicon is $\sim$12), which provides a strong screening of the Coulomb attraction. Furthermore, the electronic states are strongly delocalized in the crystalline bands (a value of r larger than the lattice spacing), leading to Coulomb potentials of the order of 10 meV and the production of Wannier excitons, which are easily dissociated with high yield at thermal energy. Thus, experimental observation measures free charge generation in response to photoexcitation in these materials. However, for carbon-based OSCs, the photogenerated electron–hole Coulomb attraction is substantially stronger ($\sim$0.5 eV) due to both their smaller dielectric constant (ε_r, $\sim$ 3) and the electronic states being localized to individual molecules instead of delocalized across the entire organic solid. The primary photoexcitation for OSCs, therefore, produces a tightly bound Frenkel exciton, a singlet excited state in which the electron and hole are still influenced by a strong Coulomb attraction. The strong Coulomb attraction creates a binding energy for the exciton that is significantly larger than the thermal energy $k_\mathrm{B}T$ [5]. The mechanism of free charge carrier generation in OSCs thus first requires the splitting of this exciton with an appreciable quantum yield. Owing to their electrically neutral nature, the motion of excitons in OSCs is unaffected by electric fields, and thus, they diffuse through the material randomly. The exciton dissociation yield is thus a critical consideration in designing a device, which converts incident radiation to free charges that can be extracted, and can range from 5 to 100 nm depending on the type of OSC selected [38–40]. This limited exciton dissociation length provides a limit on the thickness of pure material radiation

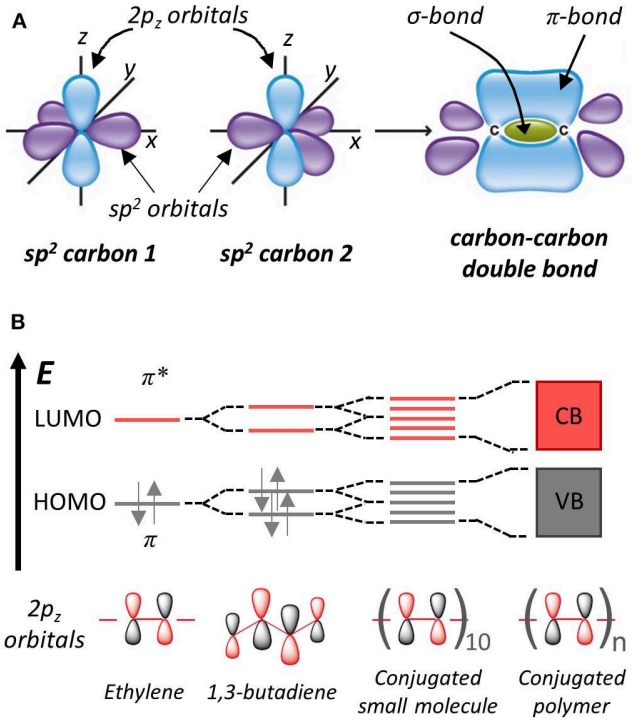

FIGURE 2 | (A) A schematic illustration of hybridized sp^2 and unhybridized $2p_z$ orbitals combining to form a σ-bond and a π-bond in a carbon–carbon double bond. **(B)** An extension of molecular orbitals to long conjugated oligomers and polymers indicating the origin of band structures (VB, valence band; CB, conduction band) in organic semiconductors.

detectors that are well-below the values typically required for substantial photon absorption, although the yield has been shown to become enhanced with an increase in the incident photon energy for some OSC materials [41]. The problem of poor photogeneration of free carriers in pure organic materials has been overcome in many electronic devices based on OSCs by the introduction of two-phase electron–donor/electron–acceptor material system, which split the exciton using the free energy difference between the respective HOMO and LUMO bands of the two materials. In such systems, the nanostructure of the two materials is critical and must be controlled to create donor/acceptor material interfaces that occur on a smaller size scale than the exciton diffusion length [42, 43].

Charge Transport

Organic materials are held together by weak Van der Waals bonds, compared to the strong coupling of inorganic molecules by covalent bonds. A consequence of the weaker bonds in OSCs is that the mean scattering length of charge carriers and the intermolecular spacing between atoms are comparable, and thus, charge transport cannot be explained using the band transport theory applied to inorganic semiconductors [44]. Instead, charge transport in OSCs is typically dominated by a phonon-assisted tunneling of charge carriers from an occupied localized state to a nearby unoccupied localized state, known as "hopping" [45]. This hopping process creates additional atomic collisions and scattering events, and consequently, the charge carrier transport in OSC materials is slower than in their inorganic semiconductor counterparts. However, it is worth noting that both the charge generation and charge transport mechanisms of OSC materials in response to ionizing radiation remain an open question, with no models currently developed to explain this behavior.

Following the creation of free charges from excitons in a radiation-sensing device, these charges must be subsequently swept out of the OSC material for detection. In the absence of an applied electric field, charge carriers will move randomly, resulting in no net movement of charge and a non-functioning electronic device. However, the application of an electric field to OSCs containing free charge carriers will accelerate the charges, which collide and scatter with defects in the semiconductor lattice to reach an average drift velocity that provides net motion through a material. The drift velocity of the carriers (υ_d) will vary depending on the electric field (E) driving carrier movement, with the proportionality constant between these two parameters given the name of the charge carrier mobility, μ [46].

$$\upsilon_d = \mu E \tag{2}$$

The mobility of an OSC material is dependent on the ability for charge carriers to tunnel between neighboring molecules without becoming trapped. Trapping can originate from a complex range of structural and electronic origins, some of which include material impurities, molecularly disordered systems, material morphologies and grain boundaries, and the nature of the charge carrier (electron or hole) [47–49]. Owing to the localized hopping mechanism and these trapping effects, OSC materials typically exhibit relatively low charge carrier mobility values of between 10^{-6} and 10^{1} cm^2 V^{-1} s^{-1}. The total drift current that is subsequently produced due to the movement of charges in the electric field (J_{drift}) is then dependent on the mobility and the total density of the charge carriers, n, produced by separating photoexcited excitons:

$$J_{drift} = e\mu nE \tag{3}$$

The carrier concentration in the device is dependent on the balance between extraction of free charges in the field and recombination of electron–hole pairs initially dissociated from excitons. This kinetic competition can be monitored on the extraction side by measurement of the mobility, while the recombination rate can be monitored by measuring the charge carrier lifetime, τ [50]. These key charge carrier processes are indicated for a typical OSC donor/acceptor system in **Figure 3**.

CONTROLLING MORPHOLOGY IN ORGANIC SEMICONDUCTING MATERIALS

The internal microstructure of OSC materials, often referred to as the material morphology, is fundamentally complex. Heterogeneities often exist across multiple length scales, from millimeter to micrometer to the subnanometer scale [51]. As discussed in the previous section, due to the reduced exciton

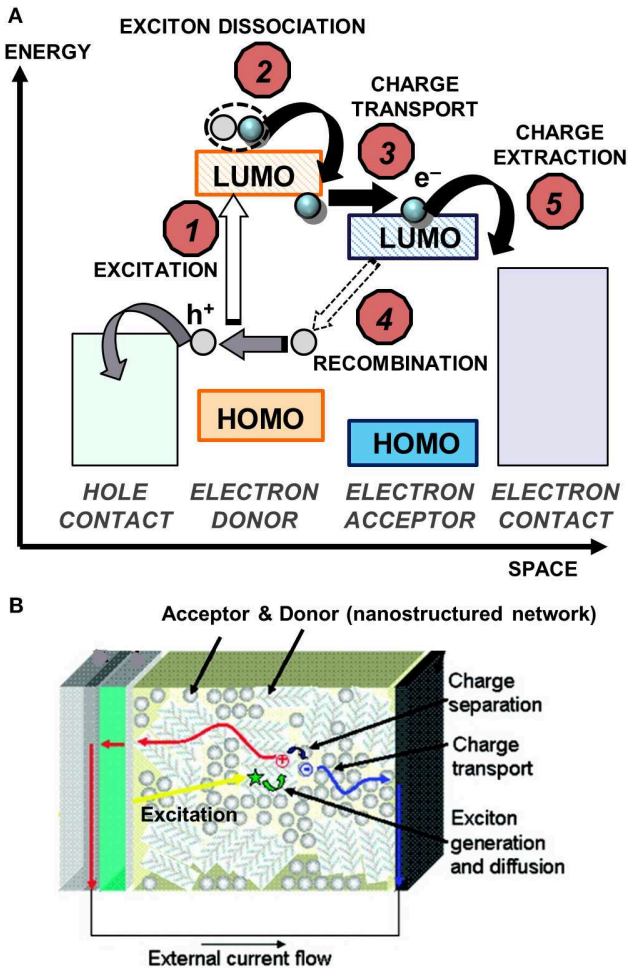

FIGURE 3 | (A) An illustration of the charge generation by photoexcitation, exciton dissociation, charge carrier transport, and recombination and extraction processes required to extract free charge after a photoexcitation event in organic semiconductor (OSC) materials. **(B)** A schematic illustration of a nanostructured network employed to promote transport and restrict recombination. Figure adapted with permission from Clarke and Durrant [37]. Copyright 2010 by American Chemical Society.

diffusion lengths in OSCs, the nanoscale morphology becomes critical in assisting efficient charge separation and transport. Understanding the unique structure–function relationships between morphology of OSC materials and device performance has been at the pinnacle of cutting-edge organic electronic materials research for the past two decades. The fundamental conundrum that has arisen is the competing demands on the optimum morphology for charge generation and transport. In a pure material, such as an OSC used for direct detection of radiation, charge transport is the key design criterion of interest. The carrier mobility in single OSC materials is highly dependent on the crystallinity, a term used to refer to the molecular ordering and alignment within a material, and thus, large aligned crystalline grains provide the optimum morphology. However, in OSC devices using the donor/acceptor blended mixture to maximize the exciton dissociation yield and enhance the charge generation, such as those employed for indirect radiation detection, a bicontinuous donor–acceptor interpenetrating network that is intimately mixed on the nanoscale and contains no large pure material crystallites is desirable [52]. Indeed, in the most sophisticated devices, these concepts can be combined to create a three-phase OSC morphology that includes amorphous and closely intermixed domains of the donor and acceptor for maximizing exciton dissociation, in addition to pure crystalline donor domains for hole transport and pure crystalline acceptor domains for electron transport [53, 54]. In this section, some key strategies to modulate the morphology of OSCs for optimizing transport and to control the nanostructure for achieving optimized charge separation and radiation detection properties will be introduced.

Tuning Crystallinity

Factors influencing the morphology of OSC films include the miscibility of the multiple semiconductors (often, donor and acceptor materials are immiscible in the solid state and cannot be blended at the nanoscale) [53, 55, 56], the physical properties of the ink deposition solvent (including boiling point, vapor pressure, and relative solubility of the donor and acceptor) [57], the nature of any coadditives for tuning ink rheology [58], thermal annealing conditions [59], and for polymer semiconductors, the glass transition temperature (T_g) [60], polymer molecular weight, and synthetic regioregularity [61].

As charge carriers are transported through π-orbital overlap of conjugated molecules in OSCs, molecular ordering (crystallinity) is critical to charge transport. An increase in the degree of crystallinity of an OSC material is a frequently applied approach to improve carrier mobility [62]. When coating OSCs from ink solutions, rapid solvent evaporation prevents the spontaneous molecular ordering toward an equilibrium morphology, instead confining molecules in kinetically trapped states [63]. To counter this, several researchers have employed a strategy of slowing the OSC crystal growth down by precipitating OSC materials from solutions with high solubility into an orthogonal solvent. Such strategies control the crystallinity and allow single crystals to be grown from solution with either p-type [64] or n-type [65] majority carriers. Such approaches have led to impressive mobility values of 10^{-2}–10^{-1} cm^2 $V^{-1}s^{-1}$ [66]. The drawback of such approaches is the slow solution growth time, which will be difficult to scale to large-area printing fabrication. However, a similar effect can be achieved with faster fabrication processing times by depositing a film with non-optimized crystallinity from one native solvent and then processing this film in a saturated environment of a second solvent to control the drying. This technique, referred to as solvent annealing, has been shown to improve OSC mobility values by several orders of magnitude [21, 67]. The printing fabrication machinery itself can also be employed to control crystallinity. Several approaches have been developed to create crystallinity in a tailored spatial dimension by induced alignment of OSC molecular chains through applied pressure in a printing device. The essence of this approach, generically known as shear-induced morphology, is to employ directional application of a printing pattern roller

in combination with a permeable membrane to simultaneously protect the otherwise free surface and induce shear flow of the blend solution in the desired regions. This approach has shown impressive control over both directional crystallinity and OSC film morphology (**Figure 4**) [68–70]. Finally, when utilizing devices with multiple OSC materials, components can preferentially segregate and diffuse toward the film/cathode or film/anode interface depending on the surface energy of the organic semiconductors in comparison with that of the underlying substrate [51, 57]. Use of judicious solvent washing, which selectively moves one of the OSC materials through the device, was shown to substantially enhance transport and photodiode performance in a photodiode using PTB7-Th as the donor and $PC_{71}BM$ as the acceptor [71]. Such an approach has also been used to selectively improve the transport properties of the n-type semiconductor in a dual OSC blend to achieve a balanced mobility of donor and acceptor materials and ensure that there is no build-up of space charge from one carrier with a significantly faster extraction process [72].

Thermal annealing of OSC materials is the other major thermodynamic handle that can be used to influence the crystallinity and morphology of the semiconductors [59, 73–75]. Perhaps, the simplest approach for tuning crystallinity in OSC materials is to cast the film from a solvent of high solubility irrespective of its drying kinetics and then thermally anneal the deposited film over time to induce the desired level of crystallinity [76]. For polymer semiconductors, the thermal treatment takes the material above its glass transition temperature, T_g, which creates thermodynamic realignment of molecular chains to induce a transition from an amorphous to a crystalline morphology. This phenomenon has been studied heavily for electronic devices based on OSC materials, with a range of advanced optical, electrical, and X-ray characterization techniques revealing that thermal annealing induces an increase in the polymer chain spacing and the coherence length of the crystallites with increasing temperature [77–80]. These crystalline domains continue to grow in size as the annealing temperature is increased up to the melting point of the polymer. Upon cooling, there is subsequent heterogeneous nucleation and a reorientation of the crystallites, which become kinetically trapped as the quasi-equilibrium structure [75]. For films and devices employing a blended OSC donor/acceptor approach to charge generation, the concept becomes more complicated. Not only does each material show independent crystallinity growth rates dependent on their individual T_g values in comparison to the annealing temperature, but the thermal treatment now also induces solid-state diffusion and a mixing or demixing of the phases depending on their enthalpic drive toward interaction [81]. It is consequently rather challenging to optimize the non-equilibrium morphology of blended OSC films through thermal annealing alone, as the film evolution kinetics are controlled by a coupled crystallization–diffusion mechanism, and thus, key morphology parameters, such as crystalline domain size, phase purity, and extent of crystallinity, cannot be varied independently [82].

Directed Nanostructure in Organic Semiconductors

Controlling OSC material nanoscale morphology across large areas during printing fabrication presents significant challenges using the crude thermodynamic levers of solvent treatments and thermal annealing [83]. One potential avenue to circumvent this challenge is to create discrete nanoparticles from the OSC materials, where the desired morphology is imprinted into the particles through chemically directed assembly using surfactants [84, 85]. Such an approach is attractive for two fundamental reasons. First, it allows the OSC nanoparticles to be removed from toxic organic solvents and dispersed into greener solvents such as water and alcohols. Furthermore, the nanoparticle approach also ensures that the thermodynamic control of the OSC film morphology is decoupled from the printing fabrication process, removing the need to consider solvent and thermal annealing treatments. Such nanoengineering approaches to building OSC devices thus enable the dual benefits of exquisite nanoscale film structure and low-cost, large-area printing of electronic devices to be simultaneously realized [86, 87].

There are two main techniques that can be employed to create organic electronic nanoparticles suspended in an aqueous solvent (or alternative non-toxic polar solvent). The first involves precipitation of a presynthesized OSC material from a solution into a non-solvent where the OSC material will crystallize in the non-solvent [88]. This method provides high-quality nanoparticulate electroactive inks; however, they are typically unstable and will form large aggregates over a time period of hours to days. Nanoparticles of donor/acceptor OSC blends synthesized via the nanoprecipitation method are reported to possess a morphology that is intimately intermixed at the nanoscale [87, 89, 90]. Such a morphology is highly beneficial for creating multiple heterointerfaces to maximize free charge generation from excitons. The second method involves creating an organic–aqueous heterophase emulsion, where the OSC materials can be transferred from their organic solutions into the aqueous phase through the use of a solubilizing molecule such as a surfactant. This emulsion method provides nanoparticulate OSC inks that are stable over time periods of months to years. Nanoparticles of OSCs synthesized via the miniemulsion method encompass various morphologies, including pristine pure semiconductors [84, 91, 92], core–shell combinations of two semiconductors [23, 93–97], and highly intermixed blends of two semiconductors [8, 98]. This morphology has been shown to be tuneable and highly dependent on the relative surface energies of the two materials [99]. Nanoparticles of OSC materials can be synthesized with customized sizes by varying the surfactant or OSC material concentrations to preset the material domain size in thin films in electronic devices. For example, the particle size can be customized between 20 and 200 nm to ensure that the crystalline domain feature size closely matches the exciton diffusion length in organic semiconductors [98, 100]. The miniemulsion method does have the drawback of leaving residual insulating surfactant embedded in an electroactive device film [86, 97]; however, recent progress has developed

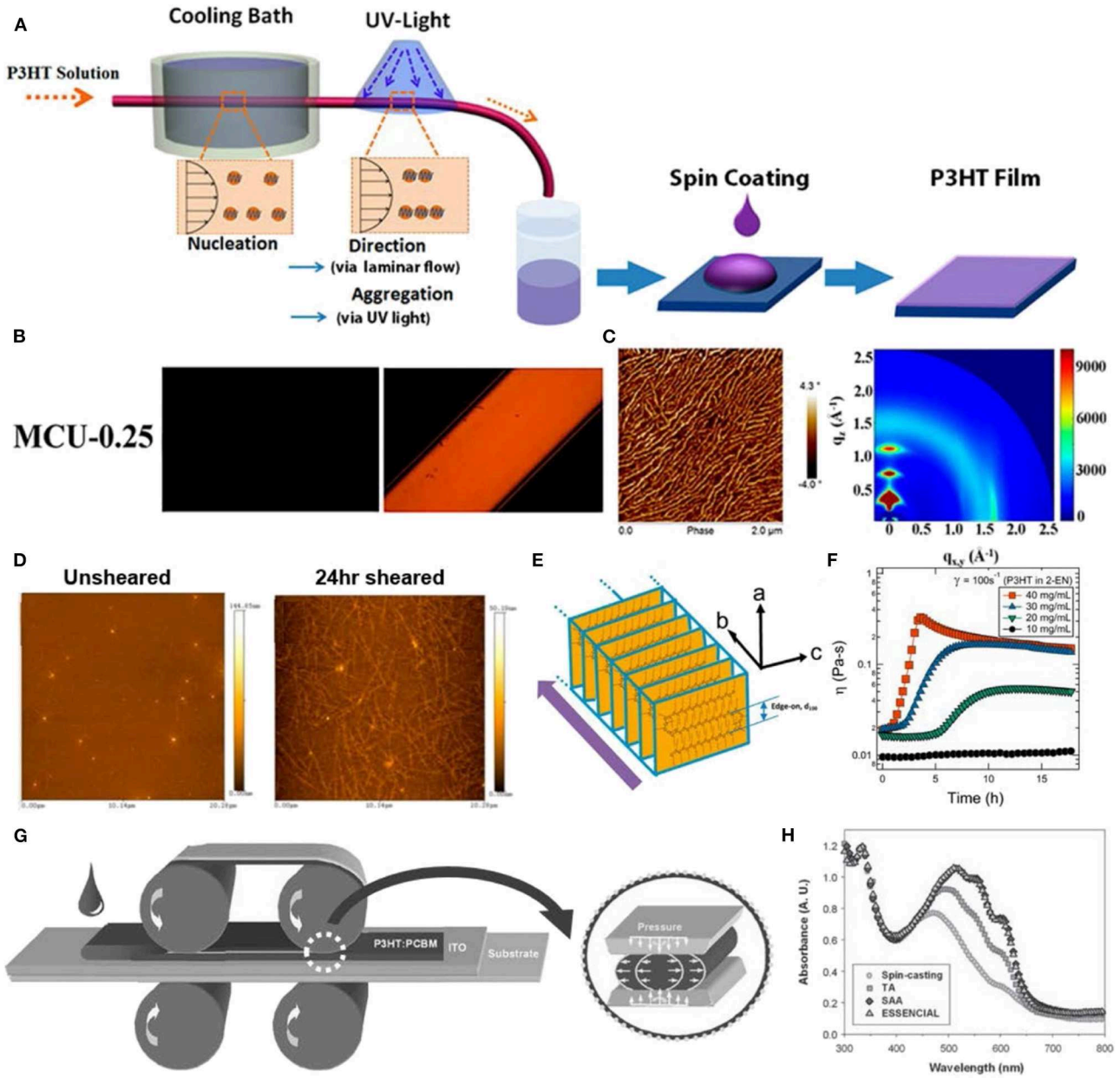

FIGURE 4 | Shear-induced polymer nucleation. **(A)** Schematic of microfluidics cooling-UV (MCU) method followed by spin coating. **(B)** Cross-polarized microscopy image of poly(3-hexylthiophene) (P3HT)/chloroform solution at the flowrate of 0.25 m/s. **(C)** Tapping-mode atomic force microscopy (AFM) phase image and grazing-incidence wide-angle X-ray scattering (GIWAXS) image of P3HT thin films on Si substrate at the optimum condition, MCU-0.25. **(D)** Tapping-mode AFM image of films spin coated from P3HT/2-ethylnaphthalene solution at 10 mg/ml under unsheared and 24 h sheared conditions. **(E)** Schematic of molecular stacking in P3HT fibrils. The arrow indicates the fibril long axis. **(F)** Change in viscosity over time under a steady shear rate of P3HT solution at various concentrations. **(G)** Schematic of roll-to-roll coating with shear denoted as ESSENCIAL. **(H)** UV-visible spectra of thin film solar cell deposited from multiple methods. Figure reproduced with permission from Qu et al. [68] (and various references contained therein). Copyright 2016 by American Chemical Society).

clever techniques to remove this surfactant using a temperature-induced critical micelle concentration switching technique that reduces the temperature of the films, causing surfactants to aggregate and be washed out of the film [90]. Recently, the OSC nanoparticle approach was employed in a novel approach to indirect radiation detection, where the scintillator was embedded into a blended nanoparticle with a donor polymer material [7]. This approach allowed the intermolecular spacing between charge carrier and radiation absorber to be brought into the realm of single nanometers, allowing all photons absorbed by the scintillator to be directly transferred to the semiconducting polymer through Förster resonance energy transfer without any

losses from scintillator emission. The study reported that the device fabricated from these blended nanoparticles exhibited impressive gamma ray detection using an all-organic radiation detection device (**Figure 5**).

PRINTED DEVICE FABRICATION

There is a strong drive toward upscaling of various OSC-based technologies such as solar cells, transistors, and sensors due to their ostensible compatibility with roll-to-roll printing. This drive toward industrial-scale prototypes and commercialization pathways has led to an increasing interest in discovering production methods that are ultimately compatible with large-scale processing [101]. The printing and coating methods for large-scale fabrication of organic electronic devices have been predominantly reported in the solar cell application arena [102–107], although increasing numbers of transistor-based devices are continuing to be reported in recent times [16, 108, 109]. Each of these technologies provides useful platforms for either the photodetector component of an indirect radiation detection system (solar cell) or a direct radiation detection system (transistor) using OSC materials printed at large scale. The major reason for the lack of progress in translating many of the OSC technologies that have been refined in highly controlled laboratory environments over the last two decades to large-scale products is the fundamentally different fabrication tools required to work on the mass manufacturing scale [33]. Consequently, the structure–function relationships that have been so carefully elucidated on the laboratory scale over decades for many of the solar cell, transistor, and sensor devices that will be described in the following section do not translate directly to the larger scale. This discrepancy explains the significant gap between the high performance of small-scale devices and the lack of larger-scale examples [63]. To bridge this "lab to fab" gap, a systematic pathway is used to transition from small-scale to roll-to-roll production environments in stages. These transitional printing stages can generally be divided into three scales: small (device area $< 1\ cm^2$), intermediate ($1\ cm^2 <$ device area $< 1\ m^2$), and large (device area $> 1\ m^2$) [101].

The small-scale approach typically investigates a transition from laboratory equipment such as spin coaters and vacuum-based small molecule and metal evaporation systems to low-cost rapid prototyping equipment such as inkjet printers and blade coaters. This fabrication scale investigates the feasibility of transferring OSC fabrication to printing and coating techniques and evaluates ink formulations and additives that will be required to transfer fabrication to larger scales [12, 110–112]. The intermediate scale employs larger-area analog procedures such as screen printing, flexographic, and gravure printing. It is at this scale that investigations into transferring some device component fabrication to roll-to-roll continuous throughput techniques are typically commenced [103, 113, 114]. Large-scale fabrication efforts use fully continuous roll-to-roll processing for all OSC device components and fabricate devices with areas of $1\ m^2$ or larger [16, 83, 115, 116]. These large-scale studies are most readily applicable to the industrial fabrication of OSC devices; however, the significant absence of such reported work in the scientific literature is indicative of the substantial capital expenditure required to purchase equipment and the complexity involved in producing functional devices where the nanoscale morphology is controlled over large size scales. Nonetheless, for OSC materials and devices to truly become ubiquitous in radiation detection, it is the research in the large-area printing space that will be required to drive this transition.

The main solution-based fabrication techniques that are compatible across each of these size scales include technologies such as slot–die coating, screen printing, flexographic printing, gravure coating, electrospraying, and inkjet printing (**Figure 6**) [103, 111, 117–121]. These techniques each have their own unique advantages and disadvantages, but all use the same principle of transferring an ink from a solution reservoir to a solid substrate using various mediums to pattern the ink deposition as desired. Flexographic, gravure, and screen printing are staple fabrication procedures in the print industry, each transferring a wet film to a substrate through a soft impression roller that applies backing pressure. The shape and layer thickness of the applied pattern are determined by the depth and density of the patterned features. Gravure contacts with a third medium. Gravure printing transfers ink from raised micropatterned features on a central roller, with a moving substrate brought into contact with the patterned features printing best suited for the fabrication of inks with a low viscosity and at very high speeds (up to 600 m/min). However, its major limitation is that substantial optimization of the ink rheology is critical, as the print quality is strongly dependent on the ink properties, the print speed, and the pressure of ink application to the substrate. Flexographic printing is a similar technique but operates through a negative imprint pattern deposition method using an additional roller. In this method, fountain rollers are utilized to continuously transfer ink from a central reservoir onto a patterned anilox roller that contains patterned microcavities embedded into the roller. This allows the collection of a metered volume of ink, which is then transferred to a third patterned printing cylinder that performs the final transfer to the substrate. Flexographic printing is most suited for processing of fine feature sizes (down to tens of micrometers) at high speeds. Screen printing, in contrast to flexographic and gravure printing, is most suited for the formation of very thick wet layers, which will dry into thick dry electroactive films. This is a suitable technique for applications requiring substantial optical thicknesses for high-energy photon absorption and films where high conductivity is required. The technique involves a squeegee blade that moves relative to a mesh screen and forces ink between openings in the mesh (which define a pattern). This technique can be employed for thicknesses in the range of 10–50 μm with suitable ink formulation viscosity [122].

Other large-scale OSC deposition methods include coating techniques that lead to a continuous wet ink layer deposited continuously along a substrate without contact between the coating head and the substrate. The coating is supplied by continuous feeding of ink to a meniscus that is standing between the coating head and the web. Such coating techniques are, therefore, zero-dimensional in the sense that no pattern is

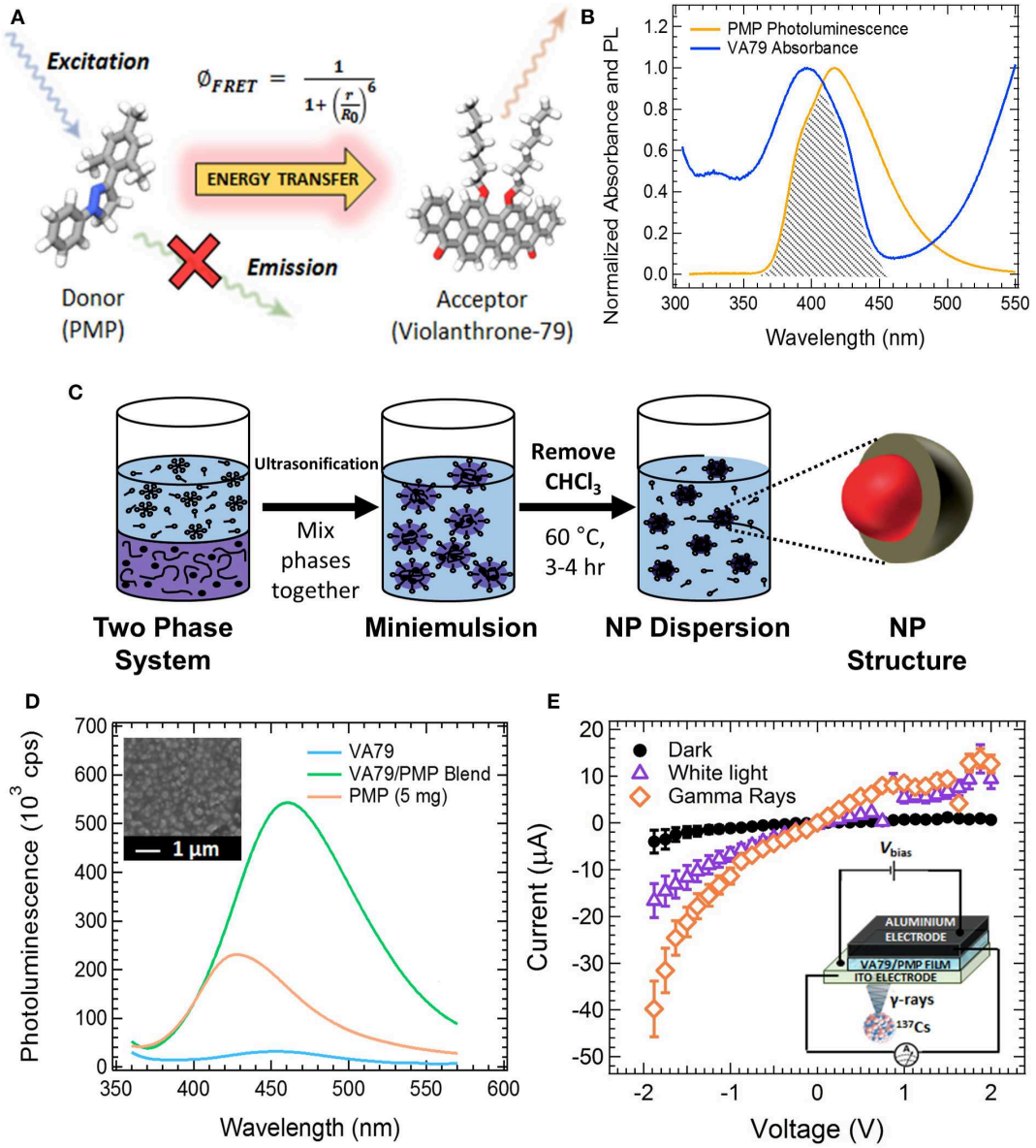

FIGURE 5 | A blended two-phase organic semiconductor (OSC) nanostructured radiation sensor. **(A)** Schematic illustration of Förster resonance energy transfer from the 1-phenyl-3-mesityl-2-pyrazoline (PMP) scintillator (donor) to the violanthrone-79 (VA79) polymer (acceptor). **(B)** Normalized spectra comparing the photoluminescence output of PMP with the absorbance spectrum of VA79. **(C)** A schematic illustration showing the process of blended OSC nanoparticle formation using the miniemulsion method. **(D)** Steady-state photoluminescence measured at an excitation wavelength of 315 nm for solid films prepared with pure VA79, pure PMP, and a VA79/PMP blend. The large growth in the output of VA79 in the presence of PMP indicates efficient Förster resonance energy transfer. The inset shows an SEM image of the nanoparticulate film structure. **(E)** Device current plotted as a function of bias voltage for sensors fabricated with a 50% mixture of VA79 and PMP. Data are shown for sensors in the dark (black circles), under illumination from a Xenon lamp (purple triangles) and under irradiation from a ^{137}Cs source (orange squares). The inset shows the radiation sensor device structure.

created, as it is simply an even coat over the substrate. Most often, however, the control of the wet thickness is far superior to any of the printing techniques, and very uniform thin layers can be prepared. The two coating techniques that have found most use thus far for roll-to-roll processing of polymer solar cells are slot–die coating and knife coating. The knife coating process has an ink reservoir before the knife that serves to supply the meniscus with new ink as it is gradually deposited behind the knife as the web passes by. In the case of slot–die coating, it is possible to coat stripes of a well-defined width along the web direction, and it is the only film forming technique that inherently allows for one-dimensional patterning. This aspect has enabled the very convincing demonstration of slot–die coating for the manufacture of polymer solar cells. In slot–die coating,

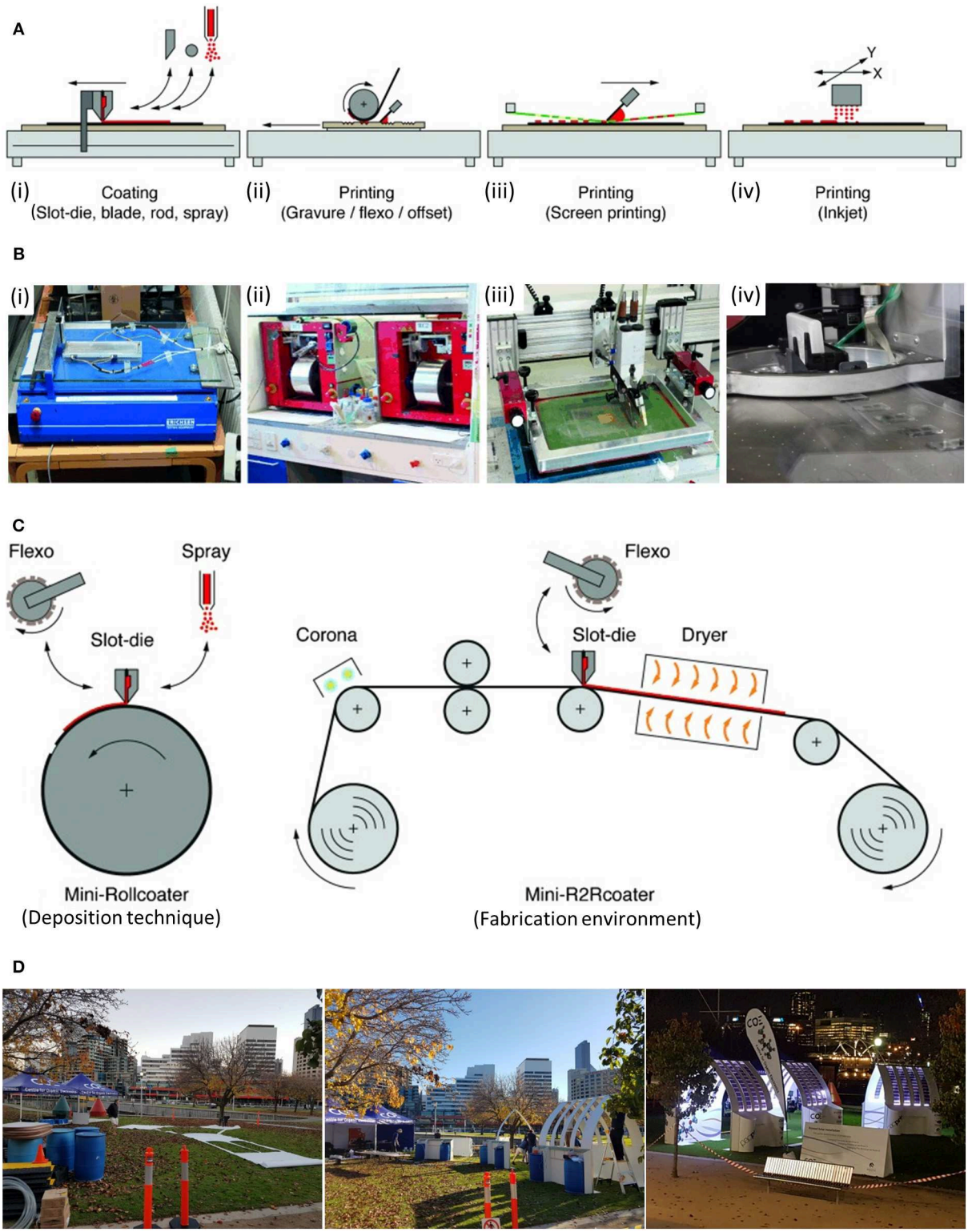

FIGURE 6 | Printing techniques and equipment for upscaling fabrication of organic semiconductor (OSC) devices. **(A)** Schematic illustrations of various printing and coating techniques that can be used for upscaling fabrication. **(B)** Photographs of laboratory equipment that match the techniques illustrated in **(A)**. **(C)** A schematic outline of an intermediate-scale roll-to-roll system for contact-free continuous deposition of OSC materials with different print techniques. Also shown is a simplified schematic of a roll-to-roll system testing inline fabrication treatments such as surface energy (corona) and thermal annealing in drying ovens. **(A–C)** Reproduced with permission from Hösel et al. [101]. Copyright 2015 by John Wiley and Sons. **(D)** Images from a recent pop-up installation of 50 m^2 of structure-integrated organic solar cells created for a demonstration in Melbourne (Australia) by researchers at the University of Newcastle.

the ink is supplied to the meniscus via a slot and a pump; it thus becomes possible to adjust the wet thickness by controlling either the speed of the web or the ink supply (or both). The natural limits to the achievable wet thicknesses depend on the coating window, which is defined not only by the ink properties and the web surface properties but also by the coating geometry.

Two final large-scale printing methods that can be used to deposit OSC electroactive inks without contact with a substrate are inkjet printing and electrospray printing. In inkjet printing, a two-dimensional pattern can be printed by specifically addressing each pixel across an area with (or without) an ink droplet. The third dimension (thickness) can, in principle, be achieved by printing multiple layers or by adding more ink to one spot. These systems are typically operated as drop-on-demand (DOD) techniques, where individual voltages are used to control droplet formation across many piezoelectric nozzles independently. In early systems, the DOD systems were limited by the achievable web speeds and resolution, but today, high-resolution systems are commercially available that are capable of fast web speeds. From an industrial point of view, inkjet printing is a relatively new processing method with some speed limitations and restrictions on ink formulations. The latter point in particular has put restraints on the use of the technology for OSC technologies. Another film forming technique is spray coating, which, like inkjet printing, achieves film formation through droplets and without physical contact between the coating head and the web. Similar to inkjet printing, the ink is applied through droplets, but where inkjet printing achieves high graphical resolution through control of the droplets, spray coating does not allow for control of the pattern and is thus inherently a zero-dimensional coating technique. It is possible to pattern through a shadow mask, but it is likely to prove impractical outside of the laboratory.

Many of these techniques have been utilized to deposit films or fabricate small-scale devices across a range of mature research fields, the breadth of which is not possible to outline in a single discussion. Instead, for further information on such research efforts, the reader is directed to recent exhaustive reviews covering progress in organic semiconductor applications including light emitting diodes [123, 124], thin-film transistors [125, 126], solar cells [127, 128], sensors [30, 129], and bioelectronics [130]. However, in terms of translating such technologies to large-scale fabrication, there has been substantially less work. Perhaps, most progress has been made in the arena of large-scale fabrication of printed organic photodiodes [15, 33, 105, 116, 131–149] and field effect or electrochemically gated transistor devices [17, 19, 29, 32, 83, 111, 150–157]. Each of these technologies provides a useful platform for the direct (transistors) or indirect (photodiode) detection of ionizing radiation using printed OSC technology, an area of research that is attracting increasing attention in recent years.

RADIATION DETECTORS FABRICATED FROM ORGANIC SEMICONDUCTORS

The application of organic materials for radiation detection has gained momentum in the past decade due to their mechanical flexibility, low cost, and simple processing, something that is not possible for inorganic solid-state devices. The effect of radiation on device photophysics has been an important concern for the performance of all organic radiation detectors; however, it remains an aspect of OSC materials that is not well-characterized. The ionizing effects depend on the absorbed dose, measured in SI units of Gray (Gy), where 1 Gy is 1 J of energy absorbed per kilogram of exposed mass. Radiation imaging corresponds to doses in the order of 0.1–1 mGy for a mammograph or chest X-ray [158]. Therefore, due to the relatively low exposure to radiation for imaging applications, much of the early research focused on these dose ranges [159–161]. The use of OSC materials for higher energy radiation detection has not been investigated as extensively due to their sensitivity to radiation damage and variation of electrical properties as a function of accumulated dose. However, in recent years, these aspects have begun to be addressed through a series of novel materials physics innovations.

Radiation Damage in Organic Semiconductors

The radiation damage of inorganic materials is well-known due to the extensive use of these devices in radiation detection, particularly for high-energy physics experiments. A study reviewing historical high-energy experimental results from the CERN (Geneva) collaboration shows that radiation damage in silicon detectors results from microscale defects that induce macroscale device effects such as a change in the depletion voltage due to the generation of defect levels in the forbidden bandgap, an increase in leakage current due to generation of, and recombination from, trap energy levels, and a decrease in charge collection efficiency due to damage-induced trapping centers [162]. However, such insights cannot be applied directly to organic materials since the charge generation and transport behavior of OSCs arise from their molecular properties and not the properties of a solid crystal. Rather, it has been shown that during exposure to radiation, OSC materials experience bond cleavage and cross-linking between molecular chains, resulting in mechanical brittleness and significantly reduced carrier transport properties [163]. The first study of irradiated OSC materials occurred for polyacetylene in 1983 [164]. The increased irradiation dose resulted in a decrease in the electrical conductivity of iodine predoped polyacetylene, although the effect was substantially greater in the undoped polymer. This result was explained by inferring that the dopant material reduced the radiation damage by capturing the ionized electron formed during photoexcitation. The same polymer was subsequently investigated for its ability to detect charged particles. Use of polyacetylene and poly(propylvinylene) (PPV) as detectors for 5 MeV alpha particles revealed that films with a thickness of 1–10 μm could detect these particles by measuring the drift velocity of charges, which are set free during the passage of a charged particle, as function of temperature, electric field, and anisotropy of the (stretched) foil. The low drift velocity (40 cm s^{-1}) made detection difficult, although stretching the polymer film induced an order of magnitude

higher drift velocity and significant charge transport anisotropy. However, the radiation hardness of these sensitive polymers was limited [165].

Further investigations into radiation hardness were conducted on polymer transistors using ion beams, with irradiation of field-effect transistors (FETs) containing an organic dielectric with 10 MeV protons at a dose of 2.85 kGy exhibiting no change in threshold voltage or off current [166]. Organic scintillator performance has also been tested using ion beams. Standard scintillators 2,5-diphenyl oxazole (PPO) and 5-bis(5-tert-butyl-2-benzoxazolyl)thiophene (BBOT) were mixed into polysiloxane matrixes and exposed to 1.8 MeV He^+ and H^+ ion beams at a flux of 1 μA cm^{-2}. Ion-beam-induced light (IBIL) emission measurements showed a loss in scintillator light yield of 70% [167]; however, the scintillators exhibited much greater radiation hardness when combined with a polyimide matrix [168]. Exposure of plastic scintillator EJ200 mixed into a poly(vinyl toluene) matrix to 6 MeV protons showed no structural damage and negligible loss-of-light emission at a dose of 0.8 MGy. However, an increase in the ion beam dose to 8 MGy induced 20% loss of scintillation performance and substantial molecular structure damage [169]. Studies on radiation hardness of organic semiconductors against high-energy neutron beams were first initiated in 1985, with the polyimide materials studied showing no change in conductivity or flexural strength after exposure to a neutron beam of flux of 10^{17} cm^{-2} ($E > 0.1$ MeV) [170]. Further examinations of carrier mobility and device performance in organic capacitors and transistors reported a drop in charge carrier mobility of 5–10% for polycarbonate capacitors exposed to a neutron flux of 10^{14} cm^{-2} ($E > 0.1$ MeV) [171]. Similar measurements using a neutron beam with flux of 10^{15} cm^{-2} s^{-1} directed onto thiophene materials poly(3-hexylthiophene) (P3HT) and PBTTT showed no loss in charge carrier mobility for PBTTT and a 65% loss in mobility for P3HT. This loss in mobility in P3HT was fully recovered upon annealing the polymer after removal of the neutron exposure [172]. Studies on mixed radiation beams composed of ions and neutrons to mimic the cosmic environment have found that materials provide a stable response in high radiation environments, making them acceptable candidates for use in harsh cosmic environments [5, 173].

Further studies in this space then transitioned from ion and neutron beams toward damage caused to OSC materials by irradiation with high-energy photons. Initially, this consisted of taking polymer photodiodes composed of P3HT photoactive layers and testing their photocurrent degradation in response to X-ray irradiation. Li et al. irradiated P3HT:PC_{61}BM devices with soft X-rays from a tungsten source (50 kV) and found an initial current drop of 46%, with a subsequent recovery to 70% of the initial performance under a total irradiation dose of 5 kGy [174]. Following on from this, Kingsley et al. irradiated P3HT:PC_{61}BM samples with high-energy X-rays from a medical linear accelerator. They found a 2% degradation in performance after 360 Gy total radiation dose for 6 MV X-rays [175] and a 5% degradation after a 500 Gy total dose for 15 MV X-rays [176]. Other polymers to be tested include poly(2-methoxy-5-(2-ethylhexyloxy)-1,4-phenylenevinylene) (MEH-PPV), where X-rays from a Mg source (12 kV) were shown to cause loss of conjugation due to oxidation [177, 178]; poly(triarylamine) (PTAA), which was shown to be stable to radiation and provide a linear output photocurrent up to a total dose of 600 Gy from a molybdenum X-ray source (50 kV) [179, 180]; and polyphenylene vinylene (PVP), where a radiation dose of 2.5 kGy from a tungsten source (40 kV) was shown to produce an enhanced charge carrier mobility and quenched photoluminescence output [181]. Interestingly, a distinct difference between OSC molecular crystals, such as sexithiophene or pentacene, and OSC polymers, such as P3HT, was observed under synchrotron X-ray irradiation with a flux density of 10^{15} photons s^{-1} mm^{-2}. The molecular crystals showed strong stability, while the polymer materials were observed to degrade and show a strong breakdown in their crystallinity and material film properties [6]. This finding suggests that these two classes of OSC materials exhibit different interaction mechanisms with ionizing radiation and will therefore be considered independently.

Organic Semiconducting Molecular Crystals

Single-crystal solids are the pinnacle of materials systems for semiconductor devices due to a combination of extremely low chemical defects, exceptional translational symmetry, and superior charge transport mobility [182]. It is perhaps unsurprising given the success of single-crystalline inorganic materials for radiation detection that researchers have shown interest in emerging OSC molecular crystals as direct replacement technologies [183]. Recent progress in growth procedures required for obtaining large-area single-crystal OSCs has enabled these materials to be explored for both indirect and direct radiation detection [184, 185]. Single-crystal growth is often performed by highly controlled physical vapor deposition procedures, which can be achieved at low temperatures and allows growth of materials on flexible plastic substrates [186–188]. However, the cost involved in depositing these materials for electronic applications in addition to the small size limits (typically of the order of 0.5–1 mm) makes such growth methods impractical for upscaling to industrially relevant fabrication. An alternative to vapor deposition is a solution-based growth method, which has the substantial advantage of compatibility with large-scale printing fabrication, as it provides a solution-processable OSC ink [189]. Initial attempts to create solution-based OSC crystals involved the slow evaporation of solvent from solutions containing dissolved OSC materials using heat and light. However, this approach was found to produce predominantly polycrystalline solids and be too slow for upscaling considerations [190, 191]. Updating this single-solvent approach, Mannsfeld et al. developed a technique to selectively grow OSC crystals by precipitating the crystals through treatment of a soluble OSC ink with an antisolvent for the semiconducting materials. They demonstrated pentacene crystals of 10–100 μm in size using this technique. Other researchers quickly adapted the two-solvent approach,

demonstrating the fabrication of molecular crystals of OSC materials including C8-BTBT [150], TIPS-pentacene [192], and 4-hydroxycyanobenzene [193]. Excitingly, these efforts were able to demonstrate macroscale crystals above 1 mm in size, with some examples exhibiting 3D anisotropically enhanced mobility and others demonstrating OSC crystals using inkjet printing fabrication. These fundamental studies demonstrate that OSC molecular crystals can be fabricated in a manner that enables high charge mobility for radiation detection while also allowing fabrication of devices that is compatible with large-scale printing.

One potential avenue for the deployment of OSC molecular crystals in radiation detection is in their use as scintillators for indirect detection systems. In particular, for neutron and gamma ray detection, liquid scintillators are often employed, as the low atomic number (Z) of the aromatic solvents helps to moderate the neutrons to thermal energy before detection with a dissolved fluorescent dye. However, fabrication of detectors using liquid scintillators must overcome issues such as the difficulty in handling, safety concerns, aggregation of the scintillating component, and difficulty in sealing the liquid. OSC molecular crystals offer a solid-state alternative that removes many of these limitations while still maintaining the low Z composition to enable efficient neutron and gamma ray detection. Examples of successful deployment of large-area OSC molecular crystal scintillators include diphenylethylene (stilbene) [194], 9,10-diphenylanthracene (DPA) [195], naphthalene, and anthracene [196]. These solution-grown OSC crystals have a series of unique features (and limitations) that will not be described in detail here but have been outlined extensively in a recent review [189].

The other major application of OSC molecular crystals is their use as the semiconducting component in direct radiation detection systems. Driven by the demand for high-quality solid crystals with a large area that can be grown at a low cost, OSC molecular crystals are an attractive alternative to inorganic semiconductors. Such inorganic semiconductors are currently limited to advanced technologies such as space exploration and state-of-the-art medical diagnostics due to the fabrication costs involved in producing high-quality materials. OSC molecular crystals are able to be fabricated from low-cost industrially relevant printing techniques [197] and, furthermore, are ideally suited to direct radiation detection due to their high charge carrier mobility and large exciton diffusion lengths, which greatly exceed those of OSC semiconducting polymers [198, 199]. Fraboni et al. have pioneered the use of OSC materials as the semiconducting component of thin film transistors for direct radiation sensing [5, 189]. Through a series of seminal papers, they have demonstrated the incorporation of a range of single-crystal OSC materials into organic thin film transistor structures that enable the direct detection of ionizing radiation at low bias voltages. These reports include OSC crystals utilizing TIPS-pentacene and rubrene [66, 200], 1,5-dinitronaphthalene (DNN) [5], anthradithiophenes [201], Parylene C [66], and 4-hydroxycyanobenzene (4HCB) [5]. Although these materials were crystallized slowly from the solution rather than fabricated with printing processes, the impressive results have shown a systematic improvement in sensitivity while consistently reducing the operating bias voltage under testing from a molybdenum X-ray source operating at 35 kV (**Figure 7**). Rubrene OSCs showed a sensitivity of 10^{-3} nC mGy^{-1} at 10 V bias, 4HCB exhibited a sensitivity of 10^{-2} nC mGy^{-1} at 400 V bias, Parylene C exhibited a sensitivity of 1.3 nC mGy^{-1} at 3 V bias, TIPS-pentacene exhibited a sensitivity of 3 nC mGy^{-1} at 3 V bias, anthradithiophene exhibited a sensitivity of 3.4 nC mGy^{-1} at 3 V bias, and DNN exhibited a sensitivity of 6 nC mGy^{-1} at 10 V bias. With improvements to the fabrication procedures, impressive OSC mobility values in the range of 10^{-1}–10^{1} cm^2 V^{-1} s^{-1} have been demonstrated, leading to new OSC crystal detectors that can be fabricated by printing, operate at bias voltages below 1 V, and produce linear responses up to 500 Gy cumulative radiation doses [200].

Semiconducting Polymers

Conjugated semiconducting polymers are the other major class of materials that have been explored for radiation detection. The major drivers for this interest are the ability to dissolve the polymers in solution, leading to deposition of the OSC active materials at high speeds through printing and coating techniques, and the ability to achieve tissue equivalency in the output response, as the detector materials are of the same elements as those found in the human body. However, their generally low carrier mobility values (10^{-3}–10^{-5} cm^2 V^{-1} s^{-1}) and poor radiation hardness present challenges for the assembly of practical radiation detectors [165]. To circumvent some of these limitations, the nanostructure of the OSC polymers can be manipulated as discussed previously [63]. However, the materials still face radiation hardness limitations and have historically been examined as disposable devices due to limited their shelf-life under irradiation from high-energy particles [1].

In general, the low atomic number of the elements in the materials typically employed in OSC technologies results in limited interactions with high-energy radiation. However, recent advancements in the deposition of thicker films ($\sim$10 μm) of PTAA have shown direct X-ray detection sensitivities of 0.3 nC mGy^{-1}, although they required applied bias values of over 100 V to achieve successful X-ray photocurrent production [177, 179, 180, 202]. While radiation damage was eventually observed, the devices showed good dose linearity responses up to dose rates of 60 mGy s^{-1}. The devices were able to be improved by incorporating a small molecule with high mobility (TIPS-pentacene) into the PTAA active layer, leading to a large enhancement in the sensitivity for direct radiation detection up to 1.2 nC mGy^{-1} [203]. One novel approach to account for radiation damage incurred by OSC polymers in direct radiation detection devices was to develop a "normally on" transistor that intentionally degrades and provides a reduced current signal in response to radiation. This approach employed P3HT as the semiconducting layer in an organic thin film transistor (OTFT) structure, where the ON/OFF ratio was reduced from a value of 3,800 without radiation down to a value of 100 after a gamma ray radiation dose of 2 kGy from a Cobalt-60 source [204].

Indirect sensitization has also been studied, typically using a P3HT:$PC_{61}BM$ donor/acceptor blend as the organic photodetecting component and a common inorganic phosphor scintillator such as terbium or europium-doped gadolinium

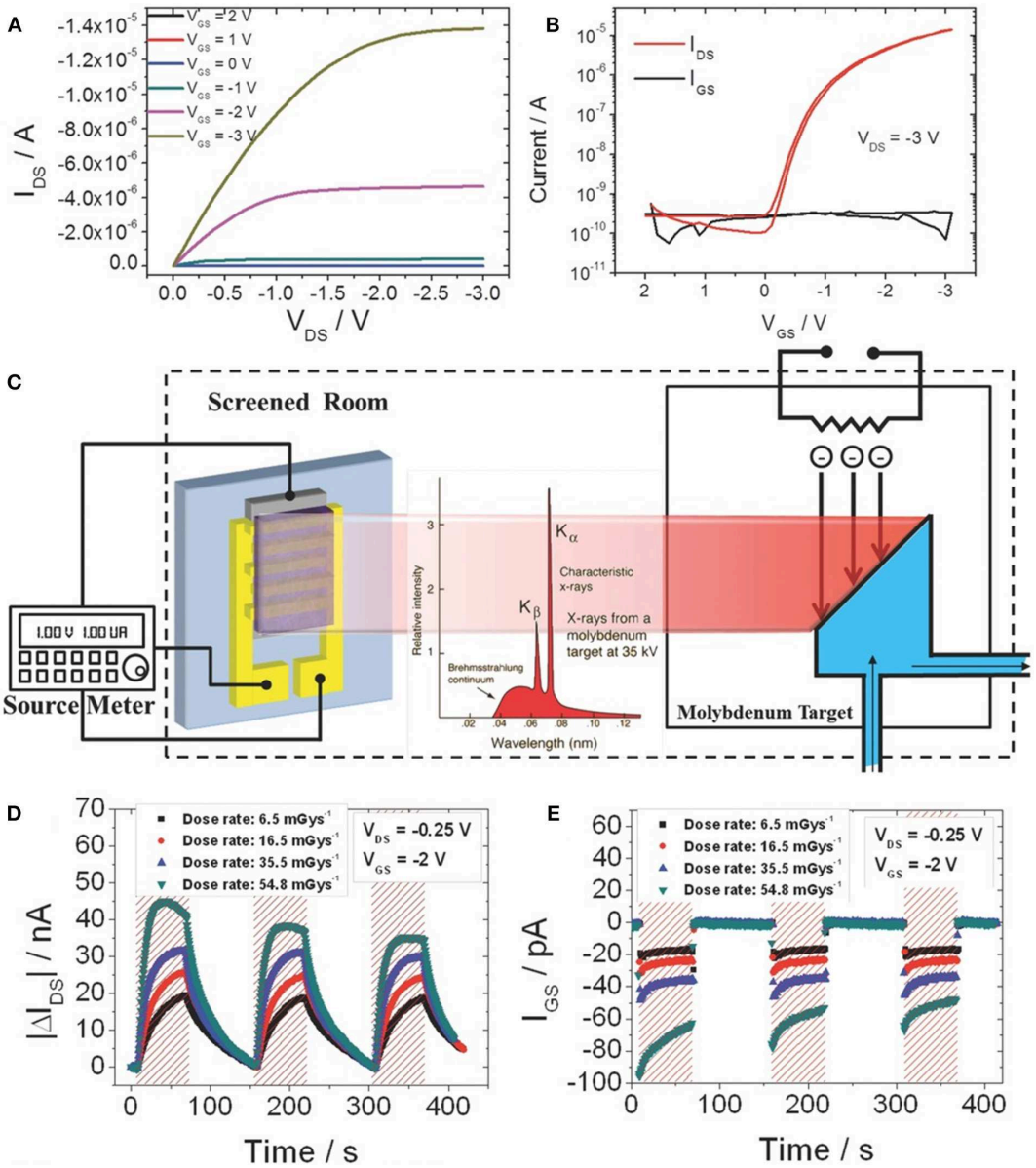

FIGURE 7 | The measured **(A)** output and **(B)** transfer characteristic curves of low-voltage organic field-effect transistor devices fabricated with a Parylene C dielectric material on plastic substrates. **(C)** Schematic representation of the measurement setup for characterization under X-rays. **(D)** The measured output response of the low-voltage organic transistor to different X-ray dose rates in the linear, and **(E)** saturation regimes of the transistor response. Reproduced with permission from John Wiley [66]. Copyright 2017 John Wiley and Sons.

oxide (GOS:Tb, GOS:Eu). Agostinelli et al. incorporated GOS:Tb into a P3HT:$PC_{61}BM$ device prepared using spin coating methods and showed a photocurrent response sensitivity of 13 nC mGy^{-1} with a bias voltage of 2 V when irradiated with 70 kV X-rays from a tungsten target. Incorporation of a distinct pure donor–pure acceptor bilayer device in place of the typical nanoscale-blended structure was able to reduce the dark current below 50 pA cm^{-2}, equivalent to values observed in existing technology in the medical imaging industry [159]. Recent work has shown that large sensitivity improvements can be made by incorporating a scintillator into devices as nanoparticles embedded into the OSC film, with reports demonstrating impressive sensitivities of 6 nC mGy^{-1} for GOS:Tb inside a P3HT:$PC_{61}BM$ organic photodiode layer [205] and 11.6 nC my^{-1} for bismuth oxide scintillator particles inside the same photodiode structure [206]. This embedded particle approach has also been used in direct detection, where embedded particles of bismuth iodide [207] and metallic tantalum [177] have been employed as high-*Z* materials to improve the radiation stopping power of thin low-*Z* OSC layers.

Excitingly, such OSC radiation detection innovations are now beginning to be translated into fabrication procedures that utilize printing to create flexible devices, with creation of a transistor structure composed of a commercial p-type semiconductor and PVP dielectric being successfully created using inkjet printing (**Figure 8**) [113]. This structure demonstrated a 93% increase in photocurrent under exposure of X-rays from a copper source (40 kV). Incorporation of printable organic (plastic) scintillators is a major advantage of OSC radiation detectors, as it allows the entire device to maintain a tissue-equivalent dosimetry response [208]. Utilization of organic scintillators PPO and POPOP into an OSC detector has demonstrated printed indirect radiation sensors fabricated on an elastomer substrate. This device exhibited only a 13% reduction in the irradiated photocurrent when the substrate was subjected to a mechanical strain of 100% [209]. Most recently, biphasic blended nanoparticles composed of an organic scintillator [1-phenyl-3-mesityl-2-pyrazoline (PMP)] and donor polymer (violanthrone-79) were fabricated, allowing photoexcited energy from gamma ray absorption to be directly transferred to the semiconducting polymer through Förster resonance energy transfer without any losses from scintillator emission. The study reported that devices fabricated from these blended nanoparticles exhibited impressive gamma ray detection sensitivity using an all-organic radiation detection device [7].

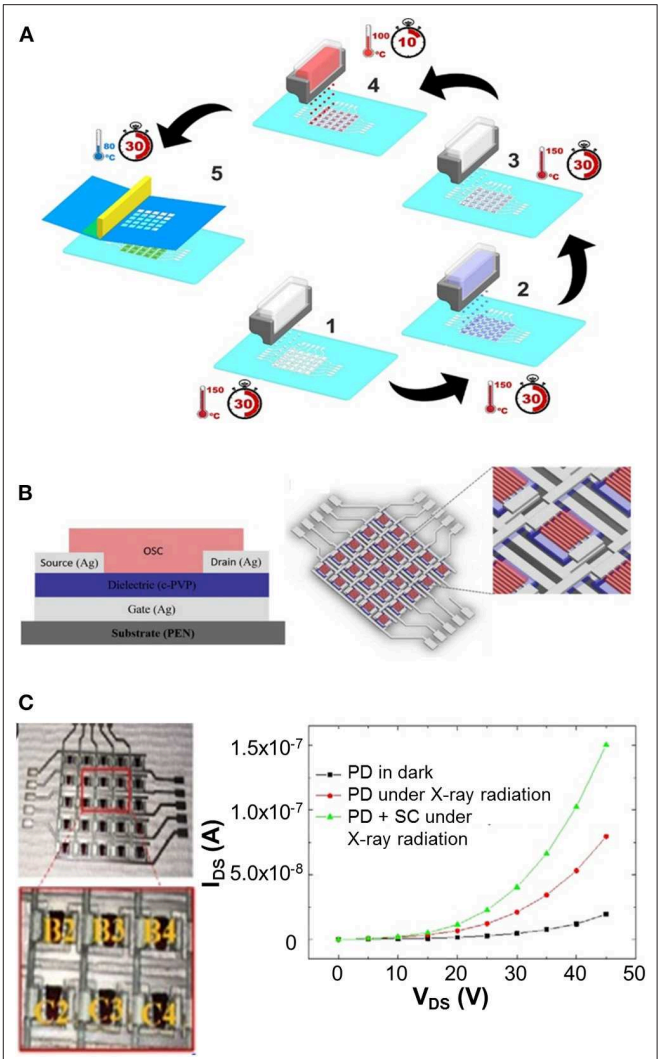

FIGURE 8 | (A) A schematic representation of the printing procedure for preparing multilayer radiation sensors composed of (1) a Ag electrode, (2) a dielectric layer (PVP), (3) Ag source and drain electrodes, (4) a semiconducting polymer layer, and (5) a scintillator ink. **(B)** A schematic image of the layer structure for both the individual radiation sensors and a 5 × 5 array prepared for imaging. **(C)** Photographs of the devices and *I–V* curves of one of the single photodiodes (PDs) present in the array in dark (black curve) and under X-ray radiation with (green curve) and without (red curve) the scintillator (SC) film. Reproduced with permission from Oliveira et al. [113]. Copyright 2018 by the American Chemical Society.

FUTURE OUTLOOK

An explosion in the number of available materials, improved functionality of materials, and sophistication of solution-based device fabrication techniques for organic semiconductors in recent years have led to considerable opportunities for the utilization of OSC materials in the detection of ionizing radiation. Such opportunities are driven by the unique readily tuneable electroactive functionality and inherent low cost of materials and fabrication offered by these carbon-based semiconductors. Although many innovative organic technologies have been developed in the laboratory for applications in solar cells, transistors, and sensors, the detection of ionizing radiation remains a relatively unexplored space. Given the well-documented nature of such radiation and its interaction with matter, there is still great uncertainty regarding the validity of transferring many fundamental discoveries pertaining to OSCs in other applications to the detection of ionizing radiation.

Consequently, there is a need to both discover and understand how the material properties of OSCs influence their interaction with ionizing radiation. Developing new structure–function relationships specific to radiation detection through advanced characterization techniques in controlled laboratory environments is a critical next step in advancing this field. Despite the relative novelty in applying OSC materials to radiation detection, there are already several promising fabrication procedures and results, such as the creation of high-mobility single-crystal OSCs, the optimization of radiation detection sensitivity through energy transfer in nanostructured films, and the tailoring of interlayer materials and thicknesses to modulate the dark current noise floor.

Controlling the nanoscale morphology of the material is already proving critical in achieving sensitive radiation detectors, with further work required to translate the high-precision laboratory fabrication procedures into the large-scale printed fabrication arena where the length scales rapidly increase. Unlocking new printing fabrication procedures for these solution processable OSC materials provides an avenue toward upscaled low-cost manufacture using roll-to-roll machinery with rapid throughput characterization performed in continuous, high-speed processes. There is still a significant amount of

fundamental research and fabrication engineering that must be developed to reveal the full potential of OSC materials in the emerging field of radiation detection. However, the existing innovations in this space already provide clear evidence that this ambition is achievable and that OSC materials will become an exciting part of the future technology portfolio in the radiation detection arena.

AUTHOR CONTRIBUTIONS

MG is the lead and senior author of the paper. He wrote the majority of the text throughout the manuscript and constructed all figures. SC and JS reviewed the literature and synthesized significant amounts of original text for the segments of work describing controlling morphology in organic semiconductors (section Controlling Morphology in Organic Semiconducting Materials) and the use of organic semiconductors in radiation detection (section Radiation Detectors Fabricated from Organic Semiconductors). JP and MP reviewed the literature and synthesized significant amounts of original text for the segments of work describing the fundamental photophysics of organic semiconductors (section Organic Semiconductors: Fundamental Photophysics) and the use of organic semiconductors in radiation detection (section Radiation Detectors Fabricated from Organic Semiconductors). They also provided substantial contributions to the editing of the manuscript.

ACKNOWLEDGMENTS

This work was performed in part at the Materials node of the Australian National Fabrication Facility, a company established under the National Collaborative Research Infrastructure Strategy to provide nano- and microfabrication facilities for Australia's researchers. The authors acknowledge funding for this work through a Strategic Investment grant from the University of Newcastle (10.32385). The authors have confirmed that any identifiable participants in this study have given their consent for publication.

REFERENCES

1. Owens A, Peacock A. Compound semiconductor radiation detectors. *Instrum Methods Phys Res Sect Accel Spectrometers Detect Assoc Equip.* (2004) **531**:18–37. doi: 10.1016/j.nima.2004.05.071
2. Anthony JE. Organic electronics: addressing challenges. *Nat Mater.* (2014) **13**:773–5. doi: 10.1038/nmat4034
3. Basirico L, Ciavatti A, Cramer T, Cosseddu P, Bonfiglio A, Fraboni B. Direct X-ray photoconversion in flexible organic thin film devices operated below 1V. *Nat Commun.* (2016) **7**:13063. doi: 10.1038/ncomms13063
4. Letourneau D, Pouliot J, Roy R. Miniature scintillating detector for small field radiation therapy. *Med Phys.* (1999) **26**:2555–61. doi: 10.1118/1.598793
5. Fraboni B, Ciavatti A, Basiricò L, Fraleoni-Morgera A. Organic semiconducting single crystals as solid-state sensors for ionizing radiation. *Faraday Discuss.* (2014) **174**:219–34. doi: 10.1039/C4FD00102H
6. Neuhold A, Novák J, Flesch HG, Moser A, Djuric T, Grodd L, et al. X-ray radiation damage of organic semiconductor thin films during grazing incidence diffraction experiments. *Nuclear Instr Meth B.* (2012) **284**:64–8. doi: 10.1016/j.nimb.2011.07.105
7. Anderson D, Cottam S, Heim H, Zhang H, Holmes NP, Griffith MJ. Printable ionizing radiation sensors fabricated from nanoparticulate blends of organic scintillators and polymer semiconductors. *MRS Commun.* (2019) **9**:1–8. doi: 10.1557/mrc.2019.132
8. Griffith MJ, Sunahara K, Furube A, Mozer AJ, Officer DL, Wagner P, et al. Cation exchange at semiconducting oxide surfaces: origin of light-induced performance increases in porphyrin dye-sensitized solar cells. *J Phys Chem C.* (2013) **117**:11885–98. doi: 10.1021/jp3067712
9. Simon DT, Gabrielsson EO, Tybrandt K, Berggren M. Organic bioelectronics: bridging the signaling gap between biology and technology. *Chem Rev.* (2016) **116**:13009–41. doi: 10.1021/acs.chemrev.6b00146
10. Owens RM, Malliaras GG. Organic electronics at the interface with biology. *MRS Bull.* (2011) **35**:449–56. doi: 10.1557/mrs2010.583
11. Hwang K, Jung Y-S, Heo Y-J, Scholes FH, Watkins SE, Subbiah J, et al. Toward large scale roll-to-roll production of fully printed perovskite solar cells. *Adv Mater.* (2015) **27**:1241–7. doi: 10.1002/adma.201404598
12. Eggenhuisen TM, Galagan Y, Biezemans AFKV, Slaats TMWL, Voorthuijzen WP, Kommeren S, et al. High efficiency, fully inkjet printed organic solar cells with freedom of design. *J Mater Chem A.* (2015) **3**:7255–62. doi: 10.1039/C5TA00540J
13. Bergqvist J, Österberg T, Melianas A, Ever Aguirre L, Tang Z, Cai W, et al. Asymmetric photocurrent extraction in semitransparent laminated flexible organic solar cells. *Flex Electron.* (2018) **2**:4. doi: 10.1038/s41528-017-0017-6
14. Seyler H, Haid S, Kwon T-H, Jones DJ, Bäuerle P, Holmes AB, et al. Continuous flow synthesis of organic electronic materials – case studies in methodology translation and scale-up. *Aust J Chem.* (2013) **66**:151–6. doi: 10.1071/CH12406
15. Carlé JE, Helgesen M, Hagemann O, Hösel M, Heckler IM, Bundgaard E, et al. Overcoming the scaling lag for polymer solar cells. *Joule.* (2017) **1**:275–89. doi: 10.1016/j.joule.2017.08.002
16. Hassinen T, Ruotsalainen T, Laakso P, Penttilä R, Sandberg HGO. Roll-to-roll compatible organic thin film transistor manufacturing technique by printing, lamination, and laser ablation. *Thin Solid Films.* (2014) **571**:212–7. doi: 10.1016/j.tsf.2014.10.086
17. Li J, Zhao Y, Tan HS, Guo Y, Di CA, Yu G, et al. A stable solution-processed polymer semiconductor with record high-mobility for printed transistors. *Sci Rep.* (2012) **2**:754. doi: 10.1038/srep00754
18. Lipomi DJ, Bao Z. Stretchable and ultraflexible organic electronics. *MRS Bull.* (2017) **42**:93–7. doi: 10.1557/mrs.2016.325
19. Griffith MJ, Cooling NA, Elkington DC, Muller E, Belcher WJ, Dastoor PC. Printable sensors for explosive detonation. *Appl Phys Lett.* (2014) **105**:143301. doi: 10.1063/1.4897140
20. Cha H, Park CE, Kwon S-K, An TK. Ternary blends to achieve well-developed nanoscale morphology in organic bulk heterojunction solar cells. *Org Electron.* (2017) **45**:263–72. doi: 10.1016/j.orgel.2017.03.028
21. Diao Y, Shaw L, Bao Z, Mannsfeld SCB. Morphology control strategies for solution-processed organic semiconductor thin films. *Energy Environ Sci.* (2014) **7**:2145–59. doi: 10.1039/C4EE00688G
22. Baran D, Ashraf RS, Hanifi DA, Abdelsamie M, Gasparini N, Rohr JA, et al. Reducing the efficiency-stability-cost gap of organic photovoltaics with highly efficient and stable small molecule acceptor ternary solar cells. *Nat Mater.* (2017) **16**:363–9. doi: 10.1038/nmat4797
23. Holmes NP, Vaughan B, Williams EL, Kroon R, Anderrson MR, Kilcoyne ALD, et al. Diketopyrrolopyrrole-based polymer:fullerene nanoparticle films with thermally stable morphology for organic photovoltaic applications. *MRS Commun.* (2017) **7**:67–73. doi: 10.1557/mrc.2017.3
24. Yin W, Dadmun M. A new model for the morphology of P3HT/PCBM organic photovoltaics from small-angle neutron scattering: rivers and streams. *ACS Nano.* (2011) **5**:4756–68. doi: 10.1021/nn200744q
25. Zhou L, He X, Lau TK, Qiu B, Wang T, Lu X, et al. Nonhalogenated solvent-processed all-polymer solar cells over 7.4% efficiency from quinoxaline-based polymers. *ACS Appl Mater Interfaces.* (2018) **10**:41318–25. doi: 10.1021/acsami.8b13949
26. Cho JH, Lee J, Xia Y, Kim B, He Y, Renn MJ, et al. Printable ion-gel gate dielectrics for low-voltage polymer thin-film

transistors on plastic. *Nat Mater.* (2008) **7**:900–6. doi: 10.1038/nmat2291
27. Elkington D, Wasson M, Belcher W, Dastoor PC, Zhou X. Printable organic thin film transistors for glucose detection incorporating inkjet-printing of the enzyme recognition element. *Appl Phys Lett.* (2015) **106**:263301. doi: 10.1063/1.4923397
28. Maasoumi F, Ullah M, Shaw PE, Li J, Burn PL, Meredith P, et al. Charge transport and recombination in heterostructure organic light emitting transistors. *Org Electron.* (2015) **25**:37–43. doi: 10.1016/j.orgel.2015.05.051
29. Someya T, Sekitani T, Iba S, Kato Y, Kawaguchi H, Sakurai T. A large-area, flexible pressure sensor matrix with organic field-effect transistors for artificial skin applications. *Proc Natl Acad Sci USA.* (2004) **101**:9966–70. doi: 10.1073/pnas.0401918101
30. Lee MY, Lee HR, Park CH, Han SG, Oh JH. Organic transistor-based chemical sensors for wearable bioelectronics. *Acc Chem Res.* (2018) **51**:2829–38. doi: 10.1021/acs.accounts.8b00465
31. Mabrook MF, Pearson C, Petty MC. Inkjet-printed polymer films for the detection of organic vapors. *IEEE Sensors J.* (2006) **6**:1435–44. doi: 10.1109/JSEN.2006.884168
32. Thompson B, Yoon H-S. Aerosol-printed strain sensor using PEDOT:PSS. *IEEE Sensors J.* (2013) **13**:4256–63. doi: 10.1109/JSEN.2013.2264482
33. Carlé JE, Helgesen M, Madsen MV, Bundgaard E, Krebs FC. Upscaling from single cells to modules–fabrication of vacuum- and ITO-free polymer solar cells on flexible substrates with long lifetime. *J Mater Chem C.* (2014) **2**:1290–7. doi: 10.1039/C3TC31859A
34. Griffith MJ, Cooling NA, Vaughan B, Elkington DC, Hart AS, Lyons AG, et al. Combining printing, coating and vacuum deposition on the roll-to-roll scale: a hybrid organic photovoltaics fabrication. *IEEE J Sel Topics Quantum Electron.* (2016) **22**:1–14. doi: 10.1109/JSTQE.2015.2487968
35. Gillespie RJ. The valence-shell electron-pair repulsion (VSEPR) theory of directed valency. *J Chem Ed.* (1963) **40**:295–301. doi: 10.1021/ed040p295
36. Atkins P, de Paula J, Keeler J. *Physical Chemistry*, 11th ed. Chicago, IL: Oxford University Press (2018).
37. Clarke TM, Durrant JR. Charge photogeneration in organic solar cells. *Chem Rev.* (2010) **110**:6736–67. doi: 10.1021/cr900271s
38. Kroeze JE, Savenije TJ, Vermeulen MJW, Warman JM. Contactless determination of the photoconductivity action spectrum, exciton diffusion length, and charge separation efficiency in polythiophene-sensitized TiO_2bilayers. *J Phys Chem B.* (2003) **107**:7696–705. doi: 10.1021/jp0217738
39. Forrest SR. The path to ubiquitous and low-cost organic electronic appliances on plastic. *Nat Commun.* (2004) **428**:911–8. doi: 10.1038/nature02498
40. Peumans P, Forrest SR. Very-high-efficiency double-heterostructure copper phthalocyanine/C60 photovoltaic cells. *Appl Phys Lett.* (2001) **79**:126–8. doi: 10.1063/1.1384001
41. Tong M, Coates NE, Moses D, Heeger AJ, Beaupré S, Leclerc M. Charge carrier photogeneration and decay dynamics in the poly (2:7-carbazole) copolymer PCDTBT and in bulk heterojunction composites with PC70BM. *Phys Rev B.* (2010) **81**:125210. doi: 10.1103/PhysRevB.81.125210
42. Riede M, Mueller T, Tress W, Schueppel R, Leo K. Small molecule solar cells - status and perspectives. *Nanotechnology.* (2008) **19**:424001. doi: 10.1088/0957-4484/19/42/424001
43. Vandewal K, Albrecht S, Hoke ET, Graham KR, Widmer J, Douglas JD, et al. Efficient charge generation by relaxed charge-transfer states at organic interfaces. *Nat Mater.* (2014) **13**:63–8. doi: 10.1038/nmat3807
44. Bässler H, Köhler A. Charge transport in organic semiconductors. *Top Curr Chem.* (2012) **312**:1–65. doi: 10.1007/128_2011_218
45. Liu C, Huang K, Park W-T, Li M, Yang T, Liu X, et al. A unified understanding of charge transport in organic semiconductors: the importance of attenuated delocalization for the carriers. *Mater Horiz.* (2017) **4**:608–18. doi: 10.1039/C7MH00091J
46. Wallace JU, Young RH, Tang CW, Chen SH. Charge-retraction time-of-flight measurement for organic charge transport materials. *Appl Phys Lett.* (2007) **91**:152104. doi: 10.1063/1.2798592
47. Armin A, Juska G, Philippa BW, Burn PL, Meredith P, White RD, et al. Doping-induced screening of the built-in-field in organic solar cells: effect on charge transport and recombination. *Adv Energy Mater.* (2013) **3**:321–7. doi: 10.1002/aenm.201200581
48. Beiley ZM, Hoke ET, Noriega R, Dacuña J, Burkhard GF, Bartelt JA, et al. Morphology-dependent trap formation in high performance polymer bulk heterojunction solar cells. *Adv Energy Mater.* (2011) **1**:954–62. doi: 10.1002/aenm.201100204
49. Mikhnenko OV, Kuik M, Lin J, van der Kaap N, Nguyen TQ, Blom PW. Trap-limited exciton diffusion in organic semiconductors. *Adv Mater.* (2014) **26**:1912–7. doi: 10.1002/adma.201304162
50. Pivrikas A, Neugebauer H, Sariciftci NS. Charge carrier lifetime and recombination in bulk heterojunction solar cells. *IEEE J Sel Topics Quantum Electron.* (2010) **16**:1746–58. doi: 10.1109/JSTQE.2010.2044978
51. Lee SS, Loo YL. Structural complexities in the active layers of organic electronics. *Annu Rev Chem Biomol Eng.* (2010) **1**:59–78. doi: 10.1146/annurev-chembioeng-073009-100851
52. Gu X, Zhou Y, Gu K, Kurosawa T, Guo Y, Li Y, et al. Roll-to-roll printed large-area all-polymer solar cells with 5% efficiency based on a low crystallinity conjugated polymer blend. *Adv Energy Mater.* (2017) **7**:1602742. doi: 10.1002/aenm.201602742
53. Ye L, Collins BA, Jiao X, Zhao J, Yan H, Ade H. Miscibility-function relations in organic solar cells: significance of optimal miscibility in relation to percolation. *Adv Energy Mater.* (2018) **8**:1703058. doi: 10.1002/aenm.201703058
54. Yu G, Gao J, Hummelen JC, Wudl F, Heeger AJ. Polymer photovoltaic cells: enhanced efficiencies via a network of internal donor-acceptor heterojunctions. *Science.* (1995) **270**:1789–91. doi: 10.1126/science.270.5243.1789
55. He X, Collins BA, Watts B, Ade H, McNeill CR. Studying polymer/fullerene intermixing and miscibility in laterally patterned films with X-ray spectromicroscopy. *Small.* (2012) **8**:1920–7. doi: 10.1002/smll.201102382
56. Collins BA, Gann E, Guignard L, He X, McNeill CR, Ade H. Molecular miscibility of polymer–fullerene blends. *J Phys Chem Lett.* (2010) **1**:3160–6. doi: 10.1021/jz101276h
57. Hansson R, Ericsson LKE, Holmes NP, Rysz J, Opitz A, Campoy-Quiles M, et al. Vertical and lateral morphology effects on solar cell performance for a thiophene–quinoxaline copolymer:PC70BM blend. *J Mater Chem A.* (2015) **3**:6970–9. doi: 10.1039/C5TA00683J
58. Liao H-C, Ho C-C, Chang C-Y, Jao M-H, Darling SB, Su W-F. Additives for morphology control in high-efficiency organic solar cells. *Materials Today.* (2013) **16**:326–36. doi: 10.1016/j.mattod.2013.08.013
59. Treat ND, Shuttle CG, Toney MF, Hawker CJ, Chabinyc ML. *In situ* measurement of power conversion efficiency and molecular ordering during thermal annealing in P3HT:PCBM bulk heterojunction solar cells. *J Mater Chem.* (2011) **21**:15224–31. doi: 10.1039/c1jm12677f
60. Müller C. On the glass transition of polymer semiconductors and its impact on polymer solar cell stability. *Chem Mater.* (2015) **27**:2740–54. doi: 10.1021/acs.chemmater.5b00024
61. Müller C, Wang E, Andersson LM, Tvingstedt K, Zhou Y, Andersson MR, et al. Influence of molecular weight on the performance of organic solar cells based on a fluorene derivative. *Adv Funct Mater.* (2010) **20**:2124–31. doi: 10.1002/adfm.201000224
62. Zhang S, Qin Y, Zhu J, Hou J. Over 14% efficiency in polymer solar cells enabled by a chlorinated polymer donor. *Adv Mater.* (2018) **30**:e1800868. doi: 10.1002/adma.201800868
63. Griffith MJ, Holmes NP, Elkington DC, Cottam S, Stamenkovic J, Kilcoyne ALD, et al. Manipulating nanoscale structure to control functionality in printed biocompatible organic electronic devices. *Nanotechnology.* (2020) **31**:092002. doi: 10.1088/1361-6528/ab57d0
64. Ciavatti A, Capria E, Fraleoni-Morgera A, Tromba G, Dreossi D, Sellin PJ, et al. Toward low-voltage and bendable X-ray direct detectors based on organic semiconducting single crystals. *Adv Mater.* (2015) **27**:7213–20. doi: 10.1002/adma.201503090
65. Katz HE, Lovinger AJ, Johnson J, Kloc C, Siegrist T, Li W, et al. A soluble and air-stable organic semiconductor with high electron mobility. *Nature.* (2000) **404**:478–81. doi: 10.1038/35006603
66. Lai S, Cosseddu P, Basiricò L, Ciavatti A, Fraboni B, Bonfiglio A. A highly sensitive, direct X-ray detector based on a low-voltage organic field-effect transistor. *Adv Electron Mater.* (2017) **3**:1600409. doi: 10.1002/aelm.201600409

67. Dickey KC, Anthony JE, Loo YL. Improving organic thin-film transistor performance through solvent-vapor annealing of solution-processable triethylsilylethynyl anthradithiophene. *Adv Mater.* (2006) **18**:1721–6. doi: 10.1002/adma.200600188
68. Qu G, Kwok JJ, Diao Y. Flow-directed crystallization for printed electronics. *Acc Chem Res.* (2016) **49**:2756–64. doi: 10.1021/acs.accounts.6b00445
69. Becerril HA, Roberts ME, Liu Z, Locklin J, Bao Z. High-performance organic thin-film transistors through solution-sheared deposition of small-molecule organic semiconductors. *Adv Mater.* (2008) **20**:2588–94. doi: 10.1002/adma.200703120
70. Park HJ, Kang MG, Ahn SH, Guo LJ. A facile route to polymer solar cells with optimum morphology readily applicable to a roll-to-roll process without sacrificing high device performances. *Adv Mater.* (2010) **22**:E247–53. doi: 10.1002/adma.201000250
71. Wang Y, Zhu H, Shi Z, Wang F, Zhang B, Dai S, et al. Engineering the vertical concentration distribution within the polymer:fullerene blends for high performance inverted polymer solar cells. *J Mater Chem A.* (2017) **5**:2319–27. doi: 10.1039/C6TA10678A
72. Zhang L, Lin B, Ke Z, Chen J, Li W, Zhang M, et al. A universal approach to improve electron mobility without significant enlarging phase separation in IDT-based non-fullerene acceptor organic solar cells. *Nano Energy.* (2017) **41**:609–17. doi: 10.1016/j.nanoen.2017.10.014
73. Sun Y, Seo JH, Takacs CJ, Seifter J, Heeger AJ. Inverted polymer solar cells integrated with a low-temperature-annealed sol-gel-derived ZnO Film as an electron transport layer. *Adv Mater.* (2011) **23**:1679–83. doi: 10.1002/adma.201004301
74. Yang X, Loos J, Veenstra SC, Verhees WJ, Wienk MM, Kroon JM, et al. Nanoscale morphology of high-performance polymer solar cells. *Nano Lett.* (2005) **5**:579–83. doi: 10.1021/nl048120i
75. Verploegen E, Mondal R, Bettinger CJ, Sok S, Toney MF, Bao Z. Effects of thermal annealing upon the morphology of polymer-fullerene blends. *Adv Funct Mater.* (2010) **20**:3519–29. doi: 10.1002/adfm.201000975
76. Ma W, Yang C, Gong X, Lee K, Heeger AJ. Thermally stable, efficient polymer solar cells with nanoscale control of the interpenetrating network morphology. *Adv Funct Mater.* (2005) **15**:1617–22. doi: 10.1002/adfm.200500211
77. Nagarjuna G, Venkataraman D. Strategies for controlling the active layer morphologies in OPVs. *J Polym Sci B.* (2012) **50**:1045–56. doi: 10.1002/polb.23073
78. Ma W, Kim JY, Lee K, Heeger AJ. Effect of the molecular weight of poly(3-hexylthiophene) on the morphology and performance of polymer bulk heterojunction solar cells. *Macromol Rapid Commun.* (2007) **28**:1776–80. doi: 10.1002/marc.200700280
79. Ballantyne AM, Chen L, Dane J, Hammant T, Braun FM, Heeney M, et al. The effect of poly(3-hexylthiophene) molecular weight on charge transport and the performance of polymer:fullerene solar cells. *Adv Funct Mater.* (2008) **18**:2373–80. doi: 10.1002/adfm.200800145
80. Gurney RS, Lidzey DG, Wang T. A review of non-fullerene polymer solar cells: from device physics to morphology control. *Rep Prog Phys.* (2019) **82**:036601. doi: 10.1088/1361-6633/ab0530
81. Treat ND, Brady MA, Smith G, Toney MF, Kramer EJ, Hawker CJ, et al. Interdiffusion of PCBM and P3HT reveals miscibility in a photovoltaically active blend. *Adv Energy Mater.* (2011) **1**:82–9. doi: 10.1002/aenm.201000023
82. Deibel C, Dyakonov V. Polymer–fullerene bulk heterojunction solar cells. *Rep Prog Phys.* (2010) **73**:095401. doi: 10.1088/0034-4885/73/9/096401
83. Pastorelli F, Schmidt TM, Hösel M, Søndergaard RR, Jørgensen M, Krebs FC. The organic power transistor: roll-to-roll manufacture, thermal behavior, and power handling when driving printed electronics. *Adv Eng Mater.* (2016) **18**:51–5. doi: 10.1002/adem.201500348
84. Holmes NP, Marks M, Cave JM, Feron K, Barr MG, Fahy A, et al. Engineering two-phase and three-phase microstructures from water-based dispersions of nanoparticles for eco-friendly polymer solar cell applications. *Chem Mater.* (2018) **30**:6521–31. doi: 10.1021/acs.chemmater.8b03222
85. Sankaran S, Glaser K, Gärtner S, Rödlmeier T, Sudau K, Hernandez-Sosa G, et al. Fabrication of polymer solar cells from organic nanoparticle dispersions by doctor blading or ink-jet printing. *Org Electron.* (2016) **28**:118–22. doi: 10.1016/j.orgel.2015.10.011
86. Ameri M, Al-Mudhaffer M, Almyahi F, Fardell GC, Marks M, Al-Ahmad A, et al. The role of stabilizing surfactant on capacitance, charge and ion transport in organic nanoparticle-based photdiodes. *ACS Appl Mater Interfaces.* (2019) **11**:10074–88. doi: 10.1021/acsami.8b19820
87. Xie C, Tang X, Berlinghof M, Langner S, Chen S, Spath A, et al. Robot-based high-throughput engineering of alcoholic polymer: fullerene nanoparticle inks for an eco-friendly processing of organic solar cells. *ACS Appl Mater Interfaces.* (2018) **10**:23225–34. doi: 10.1021/acsami.8b03621
88. Landfester K, Montenegro R, Scherf U, Güntner R, Asawapirom U, Patil S, et al. Semiconducting polymer nanospheres in aqueous dispersion prepared by a miniemulsion process. *Adv Mater.* (2002) **14**:651–5. doi: 10.1002/1521-4095(20020503)14:9<651::AID-ADMA651>3.0.CO;2-V
89. Darwis D, Holmes N, Elkington D, David Kilcoyne AL, Bryant G, Zhou X, et al. Surfactant-free nanoparticulate organic photovoltaics. *Solar Energy Mater Solar Cells.* (2014) **121**:99–107. doi: 10.1016/j.solmat.2013.10.010
90. Xie C, Heumuller T, Gruber W, Tang X, Classen A, Schuldes I, et al. Overcoming efficiency and stability limits in water-processing nanoparticular organic photovoltaics by minimizing microstructure defects. *Nat Commun.* (2018) **9**:5335. doi: 10.1038/s41467-018-07807-5
91. Gehan TS, Bag M, Renna LA, Shen X, Algaier DD, Lahti PM, et al. Multiscale active layer morphologies for organic photovoltaics through self-assembly of nanospheres. *Nano Lett.* (2014) **14**:5238–43. doi: 10.1021/nl502209s
92. Bag M, Gehan TS, Renna LA, Algaier DD, Lahti PM, Venkataraman D. Fabrication conditions for efficient organic photovoltaic cells from aqueous dispersions of nanoparticles. *RSC Adv.* (2014) **4**:45325. doi: 10.1039/C4RA07463G
93. Holmes NP, Burke KB, Sista P, Barr M, Magurudeniya HD, Stefan MC, et al. Nano-domain behaviour in P3HT:PCBM nanoparticles, relating material properties to morphological changes. *Solar Energy Mater Solar Cells.* (2013) **117**:437–45. doi: 10.1016/j.solmat.2013.06.003
94. Holmes NP, Nicolaidis N, Feron K, Barr M, Burke KB, Al-Mudhaffer M, et al. Probing the origin of photocurrent in nanoparticulate organic photovoltaics. *Solar Energy Mater Solar Cells.* (2015) **140**:412–21. doi: 10.1016/j.solmat.2015.04.044
95. Holmes NP, Marks M, Kumar P, Kroon R, Barr MG, Nicolaidis N, et al. Nano-pathways: Bridging the divide between water-processable nanoparticulate and bulk heterojunction organic photovoltaics. *Nano Energy.* (2016) **19**:495–510. doi: 10.1016/j.nanoen.2015.11.021
96. Pan X, Sharma A, Gedefaw D, Kroon R, Diaz de Zerio A, Holmes NP, et al. Environmentally friendly preparation of nanoparticles for organic photovoltaics. *Org Electron.* (2018) **59**:432–40. doi: 10.1016/j.orgel.2018.05.040
97. Al-Mudhaffer MF, Griffith MJ, Feron K, Nicolaidis NC, Cooling NA, Zhou X, et al. The origin of performance limitations in miniemulsion nanoparticulate organic photovoltaic devices. *Solar Energy Mater Solar Cells.* (2018) **175**:77–88. doi: 10.1016/j.solmat.2017.09.007
98. Marks M, Holmes NP, Sharma A, Pan X, Chowdhury R, Barr MG, et al. Building intermixed donor-acceptor architectures for water-processable organic photovoltaics. *Phys Chem Chem Phys.* (2019) **21**:5705–15. doi: 10.1039/C8CP07137C
99. Ulum S, Holmes N, Darwis D, Burke K, David Kilcoyne AL, Zhou X, et al. Determining the structural motif of P3HT:PCBM nanoparticulate organic photovoltaic devices. *Solar Energy Mater Solar Cells.* (2013) **110**:43–8. doi: 10.1016/j.solmat.2012.11.015
100. Xie C, Classen A, Späth A, Tang X, Min J, Meyer M, et al. Overcoming microstructural limitations in water processed organic solar cells by engineering customized nanoparticulate inks. *Adv Energy Mater.* (2018) **8**:1702857. doi: 10.1002/aenm.201702857
101. Hösel M, Dam HF, Krebs FC. Development of lab-to-fab production equipment across several length scales for printed energy technologies, including solar cells. *Energy Technol.* (2015) **3**:293–304. doi: 10.1002/ente.201402140
102. Søndergaard RR, Hösel M, Krebs FC. Roll-to-roll fabrication of large area functional organic materials. *J Polym Sci B.* (2013) **51**:16–34. doi: 10.1002/polb.23192
103. Krebs FC, Fyenbo J, Jørgensen M. Product integration of compact roll-to-roll processed polymer solar cell modules: methods and manufacture using flexographic printing, slot-die coating and rotary

screen printing. *J Mater Chem.* (2010) **20**:8994–9001. doi: 10.1039/c0jm01178a
104. Mulligan CJ, Wilson M, Bryant G, Vaughan B, Zhou X, Belcher WJ, et al. A projection of commercial-scale organic photovoltaic module costs. *Solar Energy Mater Solar Cells.* (2014) **120**:9–17. doi: 10.1016/j.solmat.2013.07.041
105. Machui F, Lucera L, Spyropoulos GD, Cordero J, Ali AS, Kubis P, et al. Large area slot-die coated organic solar cells on flexible substrates with non-halogenated solution formulations. *Solar Energy Mater Solar Cells.* (2014) **128**:441–6. doi: 10.1016/j.solmat.2014.06.017
106. Espinosa N, Hösel M, Angmo D, Krebs FC. Solar cells with one-day energy payback for the factories of the future. *Energy Environ Sci.* (2012) **5**:5117–32. doi: 10.1039/C1EE02728J
107. Po R, Bernardi A, Calabrese A, Carbonera C, Corso G, Pellegrino A. From lab to fab: how must the polymer solar cell materials design change? – an industrial perspective. *Energy Environ Sci.* (2014) **7**:925–43. doi: 10.1039/c3ee43460e
108. Afonso M, Morgado J, Alcácer L. Inkjet printed organic electrochemical transistors with highly conducting polymer electrolytes. *J Appl Phys.* (2016) **120**:165502. doi: 10.1063/1.4966651
109. de la Vornbrock F, Sung D, Kang H, Kitsomboonloha R, Subramanian V. Fully gravure and ink-jet printed high speed pBTTT organic thin film transistors. *Org Electron.* (2010) **11**:2037–44. doi: 10.1016/j.orgel.2010.09.003
110. Ammu S, Dua V, Agnihotra SR, Surwade SP, Phulgirkar A, Patel S, et al. Flexible, all-organic chemiresistor for detecting chemically aggressive vapors. *J Am Chem Soc.* (2012) **134**:4553–6. doi: 10.1021/ja300420t
111. Conti S, Lai S, Cosseddu P, Bonfiglio A. An inkjet-printed, ultralow voltage, flexible organic field effect transistor. *Adv Mater Technol.* (2017) **2**:4553–6. doi: 10.1002/admt.201600212
112. Yin ZP, Huang YA, Bu NB, Wang XM, Xiong YL. Inkjet printing for flexible electronics: Materials, processes and equipments. *Chin Sci Bull.* (2010) **55**:3383–407. doi: 10.1007/s11434-010-3251-y
113. Oliveira J, Correia V, Sowade E, Etxebarria I, Rodriguez RD, Mitra KY, et al. Indirect X-ray detectors based on inkjet-printed photodetectors with a screen-printed scintillator layer. *ACS Appl Mater Interfaces.* (2018) **10**:12904–12. doi: 10.1021/acsami.8b00828
114. Scheiblin G, Aliane A, Strakosas X, Curto VF, Coppard R, Marchand G, et al. Screen-printed organic electrochemical transistors for metabolite sensing. *MRS Commun.* (2015) **5**:507–11. doi: 10.1557/mrc.2015.52
115. Tong S, Yuan J, Zhang C, Wang C, Liu B, Shen J, et al. Large-scale roll-to-roll printed, flexible and stable organic bulk heterojunction photodetector. *Flex Electron.* (2017). doi: 10.1038/s41528-017-0020-y
116. Andersen TR, Cooling NA, Almyahi F, Hart AS, Nicolaidis NC, Feron K, et al. Fully roll-to-roll prepared organic solar cells in normal geometry with a sputter-coated aluminium top-electrode. *Sol Energy Mater Sol Cells.* (2016) **149**:103–9. doi: 10.1016/j.solmat.2016.01.012
117. Liu F, Ferdous S, Schaible E, Hexemer A, Church M, Ding X, et al. Fast printing and *in situ* morphology observation of organic photovoltaics using slot-die coating. *Adv Mater.* (2015) **27**:886–91. doi: 10.1002/adma.201404040
118. Zhang L, Xu X, Lin B, Zhao H, Li T, Xin J, et al. Achieving balanced crystallinity of donor and acceptor by combining blade-coating and ternary strategies in organic solar cells. *Adv Mater.* (2018) **30**:e1805041. doi: 10.1002/adma.201805041
119. Sun J, Park H, Jung Y, Rajbhandari G, Maskey BB, Sapkota A, et al. Proving scalability of an organic semiconductor to print a TFT-active matrix using a roll-to-roll gravure. *ACS Omega.* (2017) **2**:5766–74. doi: 10.1021/acsomega.7b00873
120. Ding Z, Stoichkov V, Horie M, Brousseau E, Kettle J. Spray coated silver nanowires as transparent electrodes in OPVs for Building Integrated Photovoltaics applications. *Solar Energy Mater Solar Cells.* (2016) **157**:305–11. doi: 10.1016/j.solmat.2016.05.053
121. Angmo D, Larsen-Olsen TT, Jørgensen M, Søndergaard RR, Krebs FC. Roll-to-roll inkjet printing and photonic sintering of electrodes for ITO free polymer solar cell modules and facile product integration. *Adv Mater.* (2013) **3**:172–5. doi: 10.1002/aenm.201200520
122. Chu Z, Peng J, Jin W. Advanced nanomaterial inks for screen-printed chemical sensors. *Sens Actuators B.* (2017) **243**:919–26. doi: 10.1016/j.snb.2016.12.022
123. Ho S, Liu S, Chen Y, So F. Review of recent progress in multilayer solution-processed organic light-emitting diodes. *Photonics Energy J.* (2015) **5**:057611. doi: 10.1117/1.JPE.5.057611
124. Volz D. Review of organic light-emitting diodes with thermally activated delayed fluorescence emitters for energy-efficient sustainable light sources and displays. *Photonics Energy J.* (2016) **6**:020201. doi: 10.1117/1.JPE.6.020901
125. Rivnay J, Inal S, Salleo A, Owens RM, Berggren M, Malliaras GG. Organic electrochemical transistors. *Nat Rev Mater.* (2018) **3**:17086. doi: 10.1038/natrevmats.2017.86
126. Liu D, Miao Q. Recent progress in interface engineering of organic thin film transistors with self-assembled monolayers. *Mater Chem Front.* (2018) **2**:11–21. doi: 10.1039/C7QM00279C
127. Elumalai NK, Uddin A. Open circuit voltage of organic solar cells: an in-depth review. *Energy Environ Sci.* (2016) **9**:391–410. doi: 10.1039/C5EE02871J
128. Lu L, Zheng T, Wu Q, Schneider AM, Zhao D, Yu L. Recent advances in bulk heterojunction polymer solar cells. *Chem Rev.* (2015) **15**:12666–731. doi: 10.1021/acs.chemrev.5b00098
129. Chen D, Pei Q. Electronic muscles and skins: a review of soft sensors and actuators. *Chem Rev.* (2017) **117**:11239–68. doi: 10.1021/acs.chemrev.7b00019
130. Feron K, Lim R, Sherwood C, Keynes A, Brichta A, Dastoor PC. Organic bioelectronics: materials and biocompatibility. *Int J Mol Sci.* (2018) **19:**E2382. doi: 10.3390/ijms19082382
131. Griffith MJ, Cooling NA, Vaughan B, O'Donnell KM, Al-Mudhaffer MF, Al-Ahmad A, et al. Roll-to-roll sputter coating of aluminum cathodes for large-scale fabrication of organic photovoltaic devices. *Energy Technol.* (2015) **3**:428–36. doi: 10.1002/ente.201402174
132. CHEP Press Release. *A Powerful Innovation: University of Newcastle and CHEP Sign a Partnership to Test Printed Solar Cell Panels in a Commercial Environment.* Vantage. (2017).
133. Krebs FC, Fyenbo J, Tanenbaum DM, Gevorgyan SA, Andriessen R, van Remoortere B, et al. The OE-A OPV demonstrator anno domini 2011. *Energy Environ Sci.* (2011) **4**:4116–23. doi: 10.1039/c1ee01891d
134. Krebs FC, Espinosa N, Hösel M, Søndergaard RR, Jørgensen M. 25th anniversary article: rise to power - OPV-based solar parks. *Adv Mater.* (2014) **26**:29–39. doi: 10.1002/adma.201302031
135. Larsen-Olsen TT, Søndergaard RR, Norrman K, Jørgensen M, Krebs FC. All printed transparent electrodes through an electrical switching mechanism: a convincing alternative to indium-tin-oxide, silver and vacuum. *Energy Environ Sci.* (2012) **5**:9467–71. doi: 10.1039/c2ee23244h
136. Galagan Y, Fledderus H, Gorter H, t Mannetje HH, Shanmugam S, Mandamparambil R, et al. Roll-to-roll slot–die coated organic photovoltaic (OPV) modules with high geometrical fill factors. *Energy Technol.* (2015) **3**:834–42. doi: 10.1002/ente.201500150
137. Galagan Y, Rubingh E, Andriessen R, Fan C-C, Blom PWM, Veenstra SC, et al. ITO-free flexible organic solar cells with printed current collecting grids. *Solar Energy Mater Solar Cells.* (2011) **95**:1339–43. doi: 10.1016/j.solmat.2010.08.011
138. Kaduwal D, Schleiermacher H-F, Schulz-Gericke J, Kroyer T, Zimmermann B, Würfel U. ITO-free organic solar cells with roll-to-roll coated organic functional layers from non-halogenated solvents. *Solar Energy Mater Solar Cells.* (2014) **124**:92–7. doi: 10.1016/j.solmat.2014.02.001
139. Hong S, Lee J, Kang H, Lee K. Slot-die coating parameters of the low-viscosity bulk-heterojunction materials used for polymer solarcells. *Solar Energy Mater Solar Cells.* (2013) **112**:27–35. doi: 10.1016/j.solmat.2013.01.006
140. Välimäki M, Jansson E, Korhonen P, Peltoniemi A, Rousu S. Custom-shaped organic photovoltaic modules—freedom of design by printing. *Nanoscale Res Lett.* (2017) **12**:117. doi: 10.1186/s11671-017-1871-9
141. Blankenburg L, Schultheis K, Schache H, Sensfuss S, Schrödner M. Reel-to-reel wet coating as an efficient up-scaling technique for the production of bulk-heterojunction polymer solar cells. *Solar Energy Mater Solar Cells.* (2009) **93**:476–83. doi: 10.1016/j.solmat.2008.12.013
142. Apilo P, Välimäki M, Po R, Väisänen KL, Richter H, Ylikunnari M, et al. Fully roll-to-roll printed P3HT/indene-C60-bisadduct modules with high open-circuit voltage and efficiency. *RRL Solar.* (2018) **2**:1700160. doi: 10.1002/solr.201700160

143. Lucera L, Machui F, Kubis P, Schmidt HD, Adams J, Strohm S, et al. Highly efficient, large area, roll coated flexible and rigid OPV modules with geometric fill factors up to 98.5% processed with commercially available materials. *Energy Environ Sci.* (2016) **9**:89–94. doi: 10.1039/C5EE03315B
144. Nanoflex. Available online at: http://www.nanoflexpower.com/organic (accessed September 13, 2019).
145. Optodot. Available online at: http://optodot.com/ (accessed September 13, 2019).
146. InfinityPV. Available online at: https://infinitypv.com/ (accessed September 13, 2019).
147. Leavitt N. *CSEM Brasil and SUNEW Develop Fully Transparent Solar Film Using Cambrios' ClearOhm*. Munich: Market Wired. Press Release (2017).
148. Li M, Gao K, Wan X, Zhang Q, Kan B, Xia R, et al. Solution-processed organic tandem solar cells with power conversion efficiencies >12%. *Nat Photonics.* (2017) **11**:85–90. doi: 10.1038/nphoton.2016.240
149. Berny S, Blouin N, Distler A, Egelhaaf HJ, Krompiec M, Lohr A, et al. Solar trees: first large-scale demonstration of fully solution coated, semitransparent, flexible organic photovoltaic modules. *Adv Sci.* (2016) **3**:1500342. doi: 10.1002/advs.201500342
150. Minemawari H, Yamada T, Matsui H, Tsutsumi J, Haas S, Chiba R, et al. Inkjet printing of single-crystal films. *Nature.* (2011) **475**:364–7. doi: 10.1038/nature10313
151. Fukuda K, Takeda Y, Yoshimura Y, Shiwaku R, Tran LT, Sekine T, et al. Fully-printed high-performance organic thin-film transistors and circuitry on one-micron-thick polymer films. *Nat Commun.* (2014) **5**:4147. doi: 10.1038/ncomms5147
152. Sekitani T, Takamiya M, Noguchi Y, Nakano S, Kato Y, Sakurai T, et al. A large-area wireless power-transmission sheet using printed organic transistors and plastic MEMS switches. *Nat Mater.* (2007) **6**:413–7. doi: 10.1038/nmat1903
153. Sekitani T, Noguchi Y, Zschieschang U, Klauk H, Someya T. Organic transistors manufactured using inkjet technology with subfemtoliter accuracy. *Proc Natl Acad Sci USA.* (2008) **105**:4976–80. doi: 10.1073/pnas.0708340105
154. Sekitani T, Noguchi Y, Hata K, Fukushima T, Aida T, Someya T. A rubberlike stretchable active matrix using elastic conductors. *Science.* (2008) **321**:1468–72. doi: 10.1126/science.1160309
155. Matsuhisa N, Inoue D, Zalar P, Jin H, Matsuba Y, Itoh A, et al. Printable elastic conductors by *in situ* formation of silver nanoparticles from silver flakes. *Nat Mater.* (2017) **16**:834–40. doi: 10.1038/nmat4904
156. Lochner CM, Khan Y, Pierre A, Arias AC. All-organic optoelectronic sensor for pulse oximetry. *Nat Commun.* (2014) **5**:5745. doi: 10.1038/ncomms6745
157. Griffith MJ, Willis M, Kumar P, Holdsworth JL, Bezuidenhout H, Zhou X, et al. Activation of organic photovoltaic light detectors using bend leakage from optical fibres. *ACS Appl Mater Interfaces.* (2016) **8**:7926–37. doi: 10.1021/acsami.5b12373
158. Moy J-P. Large area X-ray detectors based on amorphous silicon technology. *Thin Solid Films.* (1999) **337**:213–21. doi: 10.1016/S0040-6090(98)01179-1
159. Agostinelli T, Campoy-Quiles M, Blakesley JC, Speller R, Bradley DDC, Nelson J. A polymer/fullerene based photodetector with extremely low dark current for x-ray medical imaging applications. *Appl Phys Lett.* (2008) **93**:20. doi: 10.1063/1.3028640
160. Keivanidis PE, Greenham NC, Sirringhaus H, Friend RH, Blakesley JC, Speller R, et al. X-ray stability and response of polymeric photodiodes for imaging applications. *Appl Phys Lett.* (2008) **92**:023304. doi: 10.1063/1.2834364
161. Blakesley JC, Keivanidis PE, Campoy-Quiles M, Newman CR, Jin Y, Speller R, et al. Organic semiconductor devices for X-ray imaging. *Nuclear Instr Meth A.* (2007) **580**:774–7. doi: 10.1016/j.nima.2007.05.105
162. Lindström G, Moll M, Fretwurst E. Radiation hardness of silicon detectors – a challenge from high-energy physics. *Nuclear Instr Meth A.* (1999) **426**:1–15. doi: 10.1016/S0168-9002(98)01462-4
163. Holmes-Siedle A, Adams L. *Handbook of Radiation Effects*, 2nd ed. New York, NY: Oxford University Press (1993).
164. Yoshino K, Hayashi S, Ishii G, Inuishi Y. Electrical transport in electron beam irradiated polyacetylene. *Solid State Commun.* (1983) **46**:405–8. doi: 10.1016/0038-1098(83)90458-1
165. Beckerle P, Ströbele H. Charged particle detection in organic semiconductors. *Nuclear Instr Meth A.* (2000) **449**:302–10. doi: 10.1016/S0168-9002(00)00255-2
166. Ju S, Lee K, Janes DB, Dwivedi RC, Baffour-Awuah H, Wilkins R, et al. Proton radiation hardness of single-nanowire transistors using robust organic gate nanodielectrics. *Appl Phys Lett.* (2006) 89. doi: 10.1063/1.2336744
167. Quaranta A, Carturan S, Marchi T, Antonaci A, Scian C, Kravchuk VL, et al. Radiation hardness of polysiloxane scintillators analyzed by ion beam induced luminescence. *Nuclear Instr Meth B.* (2010) **268**:3155–9. doi: 10.1016/j.nimb.2010.05.077
168. Quaranta A. Recent developments of ion beam induced luminescence: radiation hardness study of thin film plastic scintillators. *Nuclear Instr Meth B.* (2005) **240**:117–23. doi: 10.1016/j.nimb.2005.06.098
169. Jivan H, Mellado B, Sideras-Haddad E, Erasmus R, Liao S, Madhuku M, et al. Radiation hardness of plastic scintillators for the Tile Calorimeter of the ATLAS detector. *J Phys Conf Ser.* (2015) **623**. doi: 10.1088/1742-6596/623/1/012016
170. Tucker DS, Clinard FW, Hurley GF, Fowler JD. Properties of polymers after cryogenic neutron irradiation. *J Nucl Mater.* (1985) **133–134**:805–9. doi: 10.1016/0022-3115(85)90262-4
171. Loncar B, Osmokrovic P, Vujisic M, Vasic A. Temperature and radiation hardness of polycarbonate capacitors. *J Optoelectron Adv Mater.* (2007) **9**:2863.
172. Paterno GM, Robbiano V, Fraser KJ, Frost C, Garcia Sakai V, Cacialli F. Neutron Radiation Tolerance of Two Benchmark Thiophene-Based Conjugated Polymers: the Importance of Crystallinity for Organic Avionics. *Sci Rep.* (2017) **7**:41013. doi: 10.1038/srep41013
173. Golliher EL, Pepper SV. Organic materials ionizing radiation susceptibility for the outer planet/solar probe radioisotope power source. In: *Proceeding of SPIE Intersociety Energy Conversion Engineering Conference.* (2000) CH37022. doi: 10.1109/IECEC.2000.870967
174. Li G, Yang Y, Devine RAB, Mayberry C. Radiation induced damage and recovery in poly(3-hexyl thiophene) based polymer solar cells. *Nanotechnology.* (2008) **19**:424014. doi: 10.1088/0957-4484/19/42/424014
175. Kingsley JW, Pearson AJ, Harris L, Weston SJ, Lidzey DG. Detecting 6 MV X-rays using an organic photovoltaic device. *Org Electron.* (2009) **10**:1170–3. doi: 10.1016/j.orgel.2009.06.006
176. Kingsley JW, Weston SJ, Lidzey D. Stability of X-ray detectors based on organic photovoltaic devices. *IEEE J Sel Topics Quantum Electron.* (2011) **16**:1770–5. doi: 10.1109/JSTQE.2010.2048557
177. Boroumand FA, Zhu M, Dalton AB, Keddie JL, Sellin PJ. Direct x-ray detection with conjugated polymer devices. *Appl Phys Lett.* (2007) **91**:033509. doi: 10.1063/1.2748337
178. Atreya M, Li S, Kang ET, Neoh KG, Ma ZH, Huang W. Stability studies of poly(2-methoxy-5(2′-ethyl hexyloxy)-p-(phenylene vinylene) [MEH-PPV]. *Polym Degradation Stability.* (1999) **65**:287–96. doi: 10.1016/S0141-3910(99)00018-X
179. Intaniwet A, Mills CA, Shkunov M, Thiem H, Keddie JL, Sellin PJ. Characterization of thick film poly(triarylamine) semiconductor diodes for direct x-ray detection. *J Appl Phys.* (2009) **106**:064513. doi: 10.1063/1.3225909
180. Newman CR, Sirringhaus H, Blakesley JC, Speller RD. Stability of polymeric thin film transistors for x-ray imaging applications. *Appl Phys Lett.* (2007) **91**:142105. doi: 10.1063/1.2785946
181. Graham SC, Friend RH, Fung S, Moratti SC. The effect of X-ray irradiation on poly(p-phenylene vinylene) and derivatives. *Synth Met.* (1997) **84**:903–4. doi: 10.1016/S0379-6779(96)04204-X
182. Zaitseva N, Carman L, Glenn A, Newby J, Faust M, Hamel S, et al. Application of solution techniques for rapid growth of organic crystals. *Crystal Growth J.* (2011) **314**:163–70. doi: 10.1016/j.jcrysgro.2010.10.139
183. Jiang H, Kloc C. Single-crystal growth of organic semiconductors. *MRS Bull.* (2013) **38**:28–33. doi: 10.1557/mrs.2012.308
184. Hull G, Zaitseva NP, Cherepy NJ, Newby JR, Stoeffl W, Payne SA. New organic crystals for pulse shape discrimination. *IEEE Trans Nuclear Sci.* (2009) **56**:899–903. doi: 10.1109/TNS.2009.2015944
185. Fraboni B, Ciavatti A, Merlo F, Pasquini L, Cavallini A, Quaranta A, et al. Organic semiconducting single crystals as next generation of low-cost,

room-temperature electrical X-ray detectors. *Adv Mater.* (2012) **24**:2289–93. doi: 10.1002/adma.201200283
186. Laudise RA, Kloc C, Simpkins PG, Siegrist T. Physical vapor growth of organic semiconductors. *Crystal Growth J.* (1998) **187**:449–54. doi: 10.1016/S0022-0248(98)00034-7
187. Zhang J, Wang J, Wang H, Yan D. Organic thin-film transistors in sandwich configuration. *Appl Phys Lett.* (2004) **84**:142–4. doi: 10.1063/1.1638634
188. Zhou L, Wanga A, Wu S-C, Sun J, Park S, Jackson TN. All-organic active matrix flexible display. *Appl Phys Lett.* (2006) **88**:083502. doi: 10.1063/1.2178213
189. Fraboni B, Fraleoni-Morgera A, Zaitseva N. Ionizing radiation detectors based on solution-grown organic single crystals. *Adv Mater.* (2016) **26**:2276–91. doi: 10.1002/adfm.201502669
190. Weidkamp KP, Afzali A, Tromp RM, Hamers RJ. A photopatternable pentacene precursor for use in organic thin-film transistors. *J Am Chem Soc.* (2004) **126**:12740–1. doi: 10.1021/ja045228r
191. Chen J, Tee CK, Shtein M, Martin DC, Anthony J. Controlled solution deposition and systematic study of charge-transport anisotropy in single crystal and single-crystal textured TIPS pentacene thin films. *Org Electron.* (2009) **10**:696–703. doi: 10.1016/j.orgel.2009.03.007
192. Kim YH, Yoo B, Anthony JE, Park SK. Controlled deposition of a high-performance small-molecule organic single-crystal transistor array by direct ink-jet printing. *Adv Mater.* (2012) **24**:497–502. doi: 10.1002/adma.201103032
193. Fraboni B, DiPietro R, Castaldini A, Cavallini A, Fraleoni-Morgera A, Setti L, et al. Anisotropic charge transport in organic single crystals based on dipolar molecules. *Org Electron.* (2008) **9**:974–8. doi: 10.1016/j.orgel.2008.07.006
194. Hansen W, Richter D. Determination of light output function and angle dependent correction for a stilbene crystal scintillation neutron spectrometer. *Nucl Instr Meth A.* (2002) **476**:195–9. doi: 10.1016/S0168-9002(01)01430-9
195. Zaitseva N, Glenn A, Carman L, Hatarik R, Hamel S, Faust M, et al. Pulse shape discrimination in impure and mixed single-crystal organic scintillators. *IEEE Trans Nuclear Sci.* (2011) **58**:3411–20. doi: 10.1109/TNS.2011.2171363
196. Brooks FD, Jones DTL. Directional anisotropy in organic scintillation crystals. *Nuclear Instr Meth.* (1974) **121**:69–76. doi: 10.1016/0029-554X(74)90141-4
197. Li H, Tee BC, Cha JJ, Cui Y, Chung JW, Lee SY, et al. High-mobility field-effect transistors from large-area solution-grown aligned C60 single crystals. *J Am Chem Soc.* (2012) **134**:2760–5. doi: 10.1021/ja210430b
198. Podzorov V, Menard E, Borissov A, Kiryukhin V, Rogers JA, Gershenson ME. Intrinsic charge transport on the surface of organic semiconductors. *Phys Rev Lett.* (2004) **93**:086602. doi: 10.1103/PhysRevLett.93.086602
199. Najafov H, Lee B, Zhou Q, Feldman LC, Podzorov V. Observation of long-range exciton diffusion in highly ordered organic semiconductors. *Nat Mater.* (2010) **9**:938–43. doi: 10.1038/nmat2872
200. Cosseddu P, Lai S, Barbaro M, Bonfiglio A. Ultra-low voltage, organic thin film transistors fabricated on plastic substrates by a highly reproducible process. *Appl Phys Lett.* (2012) **100**:093305. doi: 10.1063/1.3691181
201. Ciavatti A, Basiricò L, Fratelli I, Lai S, Cosseddu P, Bonfiglio A, et al. Boosting direct X-ray detection in organic thin films by small molecules tailoring. *Adv Funct Mater.* (2019) **29**:1806119. doi: 10.1002/adfm.201806119
202. Intaniwet A, Mills CA, Sellin PJ, Shkunov M, Keddie JL. Achieving a stable time response in polymeric radiation sensors under charge injection by X-rays. *ACS Appl Mater Interfaces.* (2010) **2**:1692–9. doi: 10.1021/am100220y
203. Intaniwet A, Keddie JL, Shkunov M, Sellin PJ. High charge-carrier mobilities in blends of poly(triarylamine) and TIPS-pentacene leading to better performing X-ray sensors. *Org Electron.* (2011) **12**:1903–8. doi: 10.1016/j.orgel.2011.08.003
204. Raval HN, Tiwari SP, Navan RR, Rao VR. Determining ionizing radiation using sensors based on organic semiconducting material. *Appl Phys Lett.* (2009) **94**:123304. doi: 10.1063/1.3107266
205. Büchele P, Richter M, Tedde SF, Matt GJ, Genesis Ankah N, Fischer R, et al. X-ray imaging with scintillator-sensitized hybrid organic photodetectors. *Nat Photonics.* (2015) **9**:843–8. doi: 10.1038/nphoton.2015.216
206. Thirimanne HM, Jayawardena K, Parnell AJ, Bandara R, Karalasingam A, Pani S, et al. High sensitivity organic inorganic hybrid X-ray detectors with direct transduction and broadband response. *Nat Commun.* (2018) **9**:2926. doi: 10.1038/s41467-018-05301-6
207. Wang Y, Herron N. X-ray photoconductive nanocomposites. *Science.* (1996) **273**:632–4. doi: 10.1126/science.273.5275.632
208. Takada E, Fujii K, Imai H, Okada H, Namito Y, Nakamura T. Response of organic photodiode fabricated directly on plastic scintillator to X-rays. *J Nuclear Sci Tech.* (2014) **52**:104–8. doi: 10.1080/00223131.2014.933135
209. Oliveira J, Correia V, Costa P, Francesko A, Rocha G, Lanceros-Mendez S. Stretchable scintillator composites for indirect X-ray detectors. *Composites Part B Eng.* (2018) **133**:226–31. doi: 10.1016/j.compositesb.2017.09.031

Conflict of Interest: The authors declare that the research was conducted in the absence of any commercial or financial relationships that could be construed as a potential conflict of interest.